Defense Presentation

Failure Processes in Soft and Quasi-Brittle Materials with Nonhomogeneous Microstructures

Daniel Spring

Department of Civil and Environmental Engineering
University of Illinois at Urbana-Champaign

May 22nd, 2015

NSERC CRSNG

ILLINOIS
UNIVERSITY OF ILLINOIS AT URBANA-CHAMPAIGN

Committee Members

Prof. Glaucio H. Paulino (Chair, CEE GaTech/UIUC)
Prof. Iwona Jasiuk (MechSE UIUC)
Prof. William G. Buttlar (CEE UIUC)
Prof. Oscar Lopez-Pamies (CEE UIUC)
Prof. Ahmed E. Elbanna (CEE UIUC)
Prof. Kyoungsoo Park (CEE Yonsei)

Fracture and Failure is Prevalent in Materials Science and Across the Engineering Disciplines

Materials (Soft)

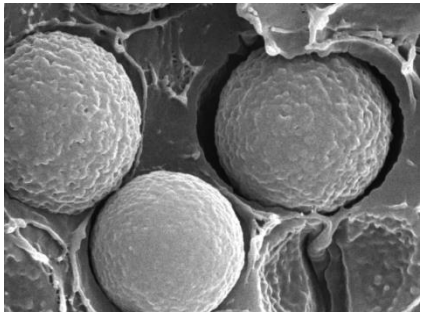

Renner, 2010

Materials (Quasi-Brittle)

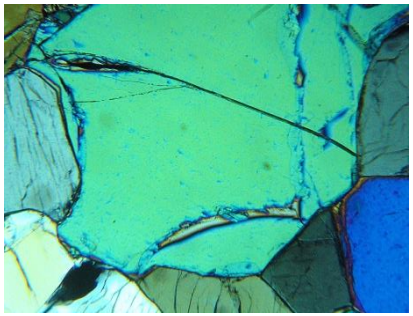

und.nodak.com

Biomechanical

pixshark.com

Structural

imrtest.com

Earthquake

usgs.gov

Geomechanical

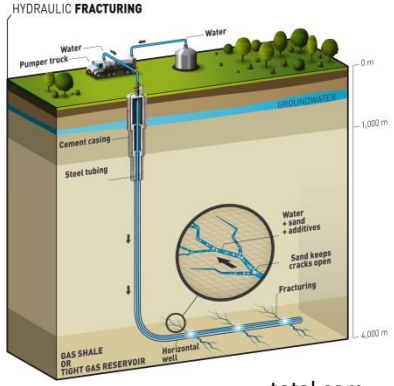

total.com

The overarching theme of my research is to develop computational tools and techniques to investigate problems in the fields of materials science and computational fracture mechanics.

Presentation Structure

1. Perfectly Bonded Interphases in Particle Reinforced Elastomers

- Goudarzi T, **Spring DW**, Paulino GH, Lopez-Pamies O, Filled elastomers: A theory of filler reinforcement based on hydrodynamic and interphasial effects. *Journal of the Mechanics and Physics of Solids*, Vol. 80, pp. 37-67, 2015.

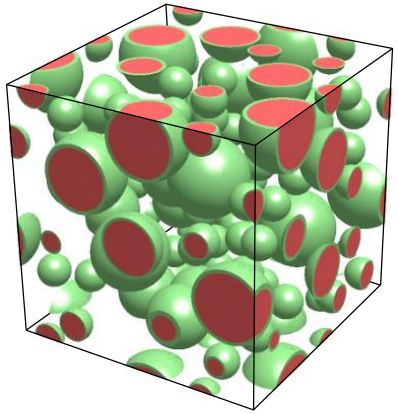

2. Interfacial Debonding in Particle Reinforced Elastomers

- **Spring DW**, Paulino GH, A growing library of three-dimensional cohesive elements for use in ABAQUS. *Engineering Fracture Mechanics*, Vol. 126, pp. 190-216, 2014.
- **Spring DW**, Paulino GH, Computational homogenization of the debonding of particle reinforced elastomers: The role of interphases in interfaces. *Under Review.*

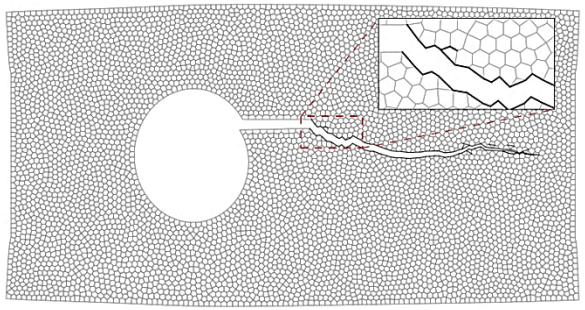

3. Reducing Mesh Bias in Dynamic Fracture Simulations Through Adaptive Operators

- Leon SE, **Spring DW**, Paulino GH, Reduction in mesh bias for dynamic fracture using adaptive splitting of polygonal finite elements. *International Journal for Numerical Methods in Engineering*, Vol. 100, pp. 555-576, 2014.
- **Spring DW**, Leon SE, Paulino GH, Unstructured polygonal meshes with adaptive refinement for the numerical simulation of dynamic cohesive fracture. *International Journal of Fracture*, Vol. 189, pp. 33-57, 2014.

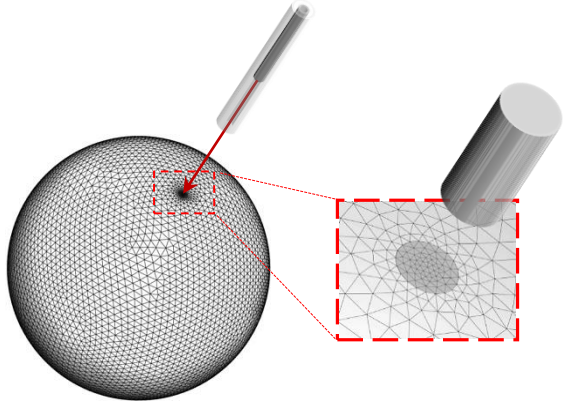

4. Regularizing Pervasive Fracture and Fragmentation Behavior in Three-Dimensions

- **Spring DW**, Paulino GH, Numerical unstructuring as a means for achieving pervasive fracture and fragmentation in three-dimensions. *In Preparation*.

Seemingly Similar Composites Can Display Remarkably Different Behavior

Effective Modulus
(small deformations)

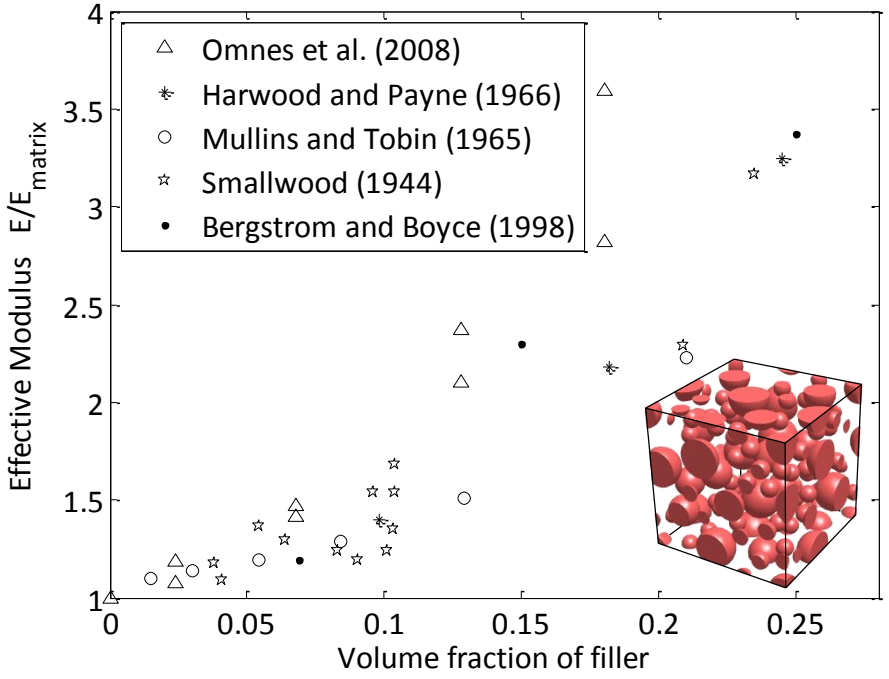

Constitutive Response
(large deformations)

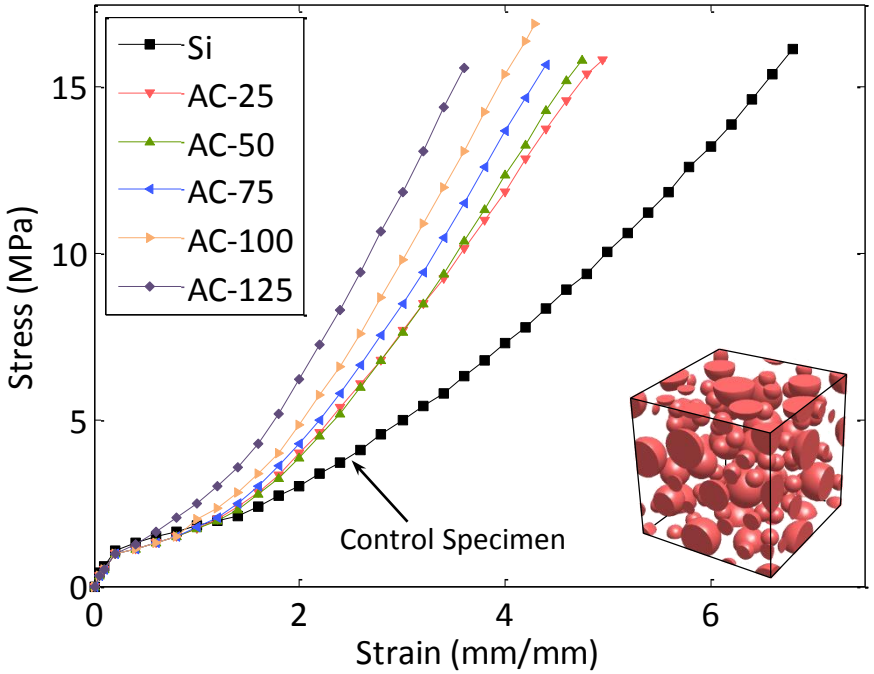

Bergström JS, Boyce MC, Mechanical behavior of particle filled elastomers, *Rubber Chemistry and Technology*, vol. 72, pp. 633-656, 1998.

Ramier J, Chazeau L, Gauthier C, Influence of silica and its different surface treatments on the vulcanization process of silica filled SBR, *Rubber Chemistry and Technology*, vol. 80, pp. 183-193, 2007.

Ramier J, Comportement mécanique d'élastomères chargés, influence de l'adhésion charge – polymère, influence de la morphologie. PhD Dissertation, L'Institut National des Sciences Appliquées de Lyon, 2004.

Inclusions Tend to Restrict Polymer Chain Mobility

When a particle is embedded in an elastomer, the polymer chains in the elastomer tend to anchor onto the surface of the particle.

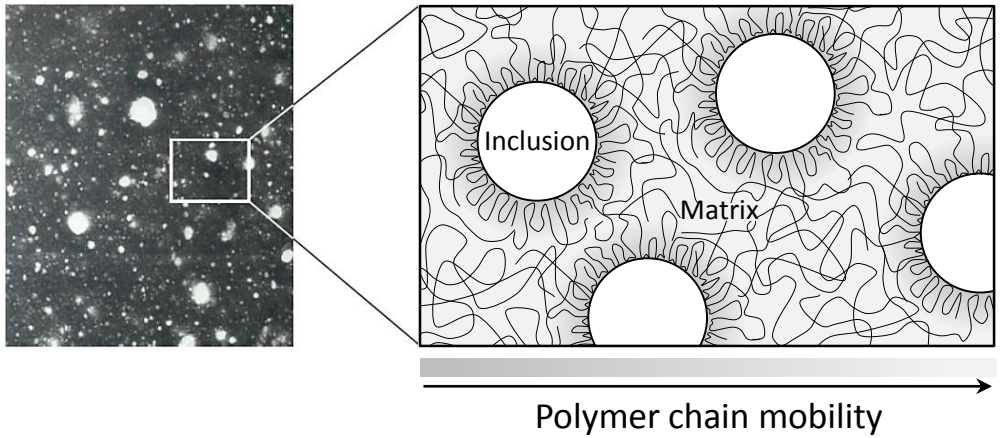

The effective modulus of the elastomer in the vicinity of the particles can be on the order of ten times greater than that in the bulk of the elastomer.

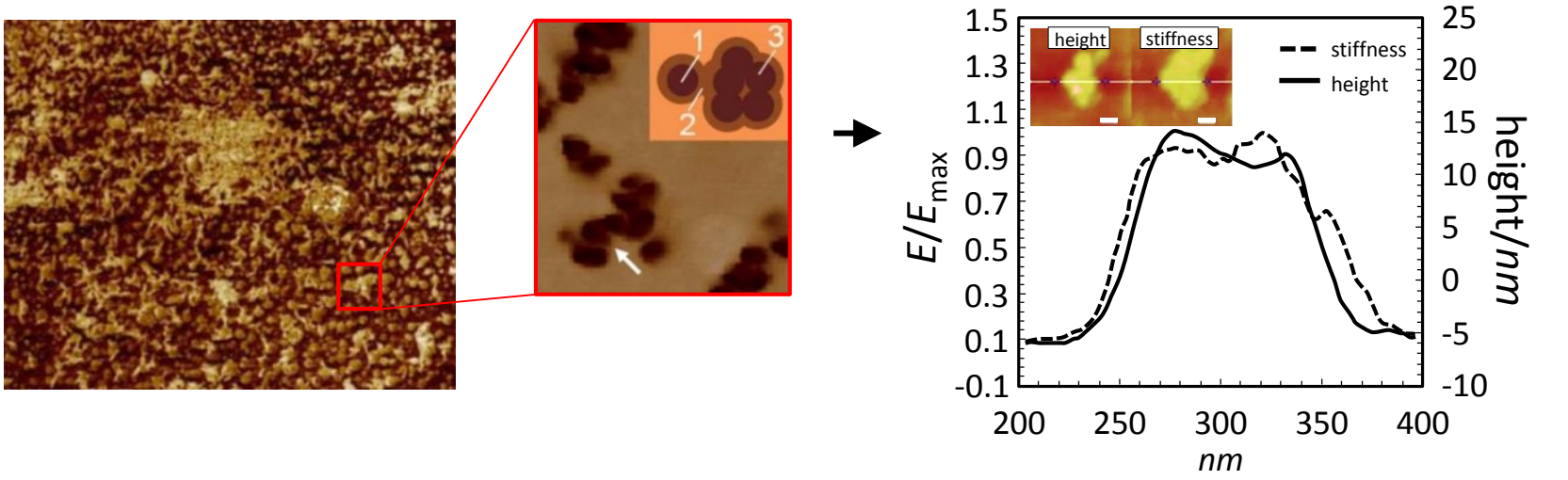

Qu M, Deng F, Kalkhoran SM, Gouldstone A, Robisson A, Van Vliet KJ, 2011. Nanoscale visualization and multiscale mechanical implications of bound rubber interphases in rubber-carbon black nanocomposites. *Soft Matter*. Vol. 7, pp. 1066-1077.

A Computational Framework Using RUCs

- Particles and their associated interphases are placed within the microstructure in a random, periodic manner, using random sequential adsorption.
- We consider both **monodisperse** and **polydisperse** distributions of particles.

30 monodisperse particles

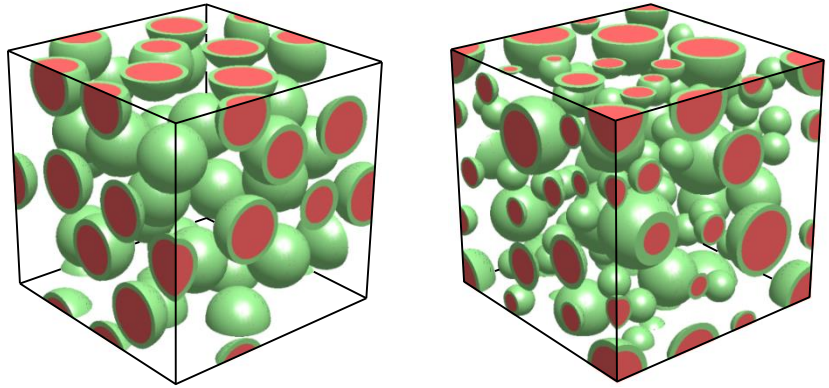

80 polydisperse particles

- The particles are placed in such a manner that the microstructure is periodic.

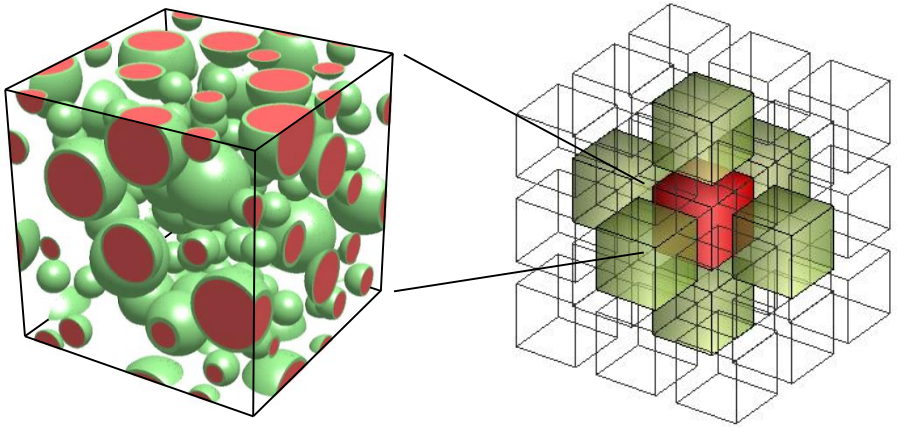

Goudarzi T, Spring DW, Paulino GH, Lopez-Pamies O, Filled elastomers: A theory of filler reinforcement based on hydrodynamic and interphasial effects. *Journal of the Mechanics and Physics of Solids*, Vol. 80, pp. 37-67, 2015

Algorithm for Constrained Random Particle Placement

- Particle sizes are prescribed and their locations are selected in a random but constrained manner.

	Monodisperse	Polydisperse
Particle radii	$r = L\left(\frac{3c_p}{4\pi N}\right)^{1/3}$	$\left\{r^{(1)}, r^{(2)}, r^{(3)}\right\} \cong \left\{r, \frac{7}{9}r, \frac{4}{9}r\right\}$ $\left\{c_p^{(1)}, c_p^{(2)}, c_p^{(3)}\right\} \cong \left\{\frac{1}{2}c_p, \frac{1}{4}c_p, \frac{1}{4}c_p\right\}$
Interphase Thickness	$\frac{t}{r} = \left(1+\frac{c_i}{c_p}\right)^{1/3} - 1$	$\left\{\frac{t^{(1)}}{r^{(1)}}, \frac{t^{(2)}}{r^{(2)}}, \frac{t^{(3)}}{r^{(3)}}\right\} = \left\{\frac{t}{r}, \frac{t}{r}, \frac{t}{r}\right\}$
Center-to-center distance between particles	$\left\|\mathbf{X}^i - \mathbf{X}^j - \mathbf{h}\right\| \geq 2\left(r+t\right)\left(1+d_1\right)$	$d_1 \geq 0.03$
Distance between particle and boundary	$\left\|X_a^i - r - t\right\| \geq d_2\left(r+t\right)$ $\left\|X_a^i + r + t - L\right\| \geq d_2\left(r+t\right)$	$d_2 = 0.05$

Feder J, 1980. Random sequential adsorption. *Journal of Theoretical Biology*, Vol. 87, pp. 237–254.

Goudarzi T, Spring DW, Paulino GH, Lopez-Pamies O, Filled elastomers: A theory of filler reinforcement based on hydrodynamic and interphasial effects. *Journal of the Mechanics and Physics of Solids*, Vol. 80, pp. 37-67, 2015

Discretization and Isotropy Assessment

- A mesh containing approximately $200{,}000$ bulk elements is used to discretize the domain.

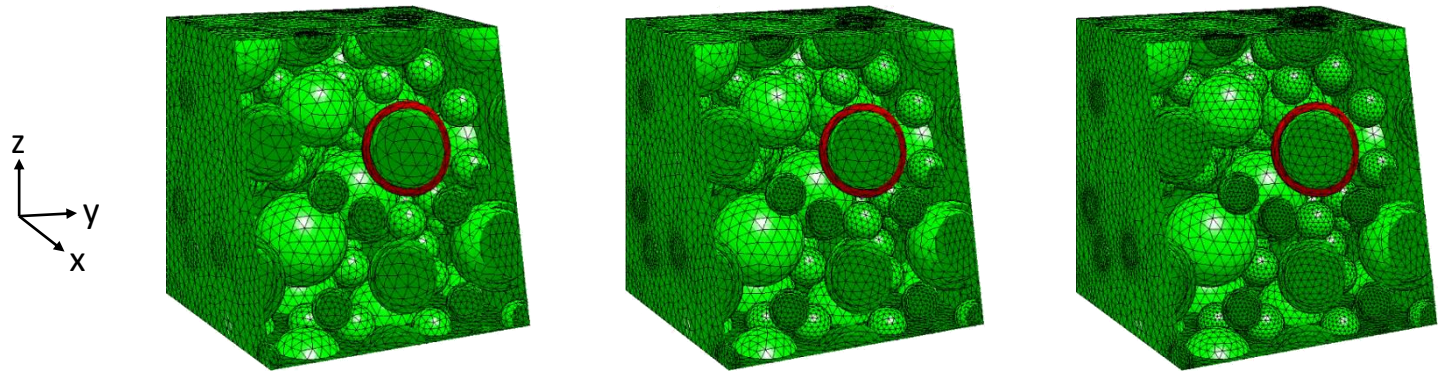

100,000 elements 200,000 elements 300,000 elements

- We use a sufficient constitutive approach to assess the isotropy of the microstructures. In an isotropic material, the average Cauchy stress tensor, $\bar{\boldsymbol{\sigma}} = \bar{\mathbf{S}}\bar{\mathbf{F}}^{\mathrm{T}}$ and average left Green-Cauchy strain tensor $\bar{\mathbf{B}} = \bar{\mathbf{F}}\bar{\mathbf{F}}^{\mathrm{T}}$ are coaxial, where:

$$\bar{\mathbf{F}} = \sum_{i}^{N_{elem}} \frac{V_i}{V_\Omega} \mathbf{F}_{elem} \qquad \bar{\mathbf{S}} = \sum_{i}^{N_{elem}} \frac{V_i}{V_\Omega} \mathbf{S}_{elem}$$

The angle between the principal axes of the stress and strain measures are zero for a purely isotropic material, and should be close to zero for the RUCs we consider.

Schröberl J, 1997. NETGEN - an advancing front 2D/3D-mesh generator based on abstract rules. *Computing and Visualization in Science*, Vol. 1, pp. 41–52.

Goudarzi T, Spring DW, Paulino GH, Lopez-Pamies O, Filled elastomers: A theory of filler reinforcement based on hydrodynamic and interphasial effects. *Journal of the Mechanics and Physics of Solids*, Vol. 80, pp. 37-67, 2015

Representative Polydisperse Microstructures

	No Interphase	$t/r_p = 0.1$	$t/r_p = 0.2$
$c_p = 10\%$	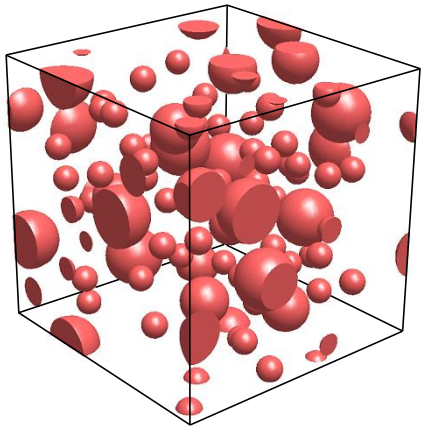	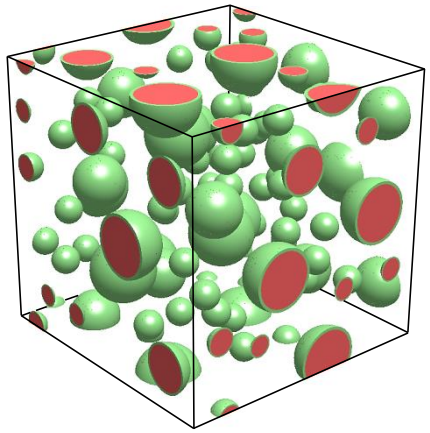	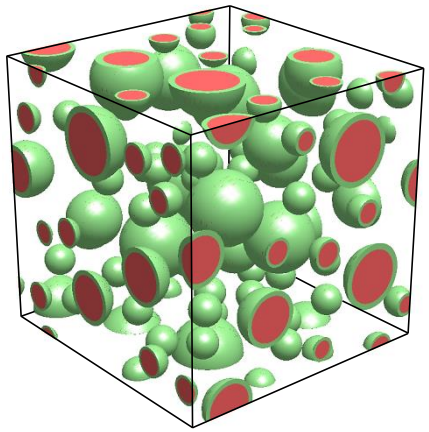
$c_p = 20\%$	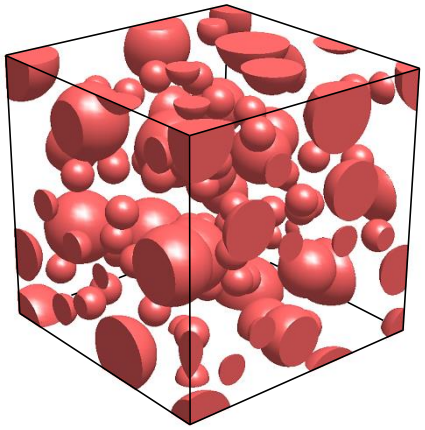	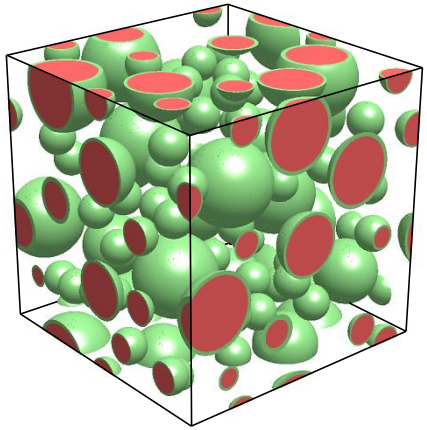	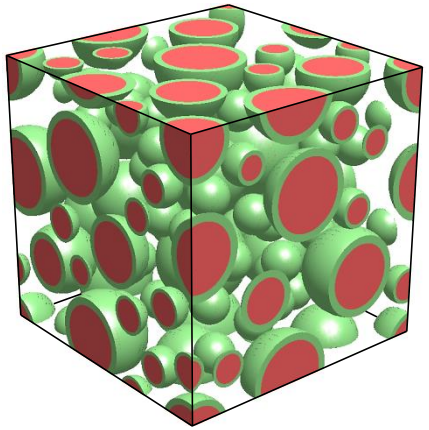

Daniel W. Spring. “Failure Processes in Soft and Quasi-Brittle Materials with Nonhomogeneous Microstructures.” PhD Dissertation, Department of Civil and Environmental Engineering, UIUC, 2015.

Verification with Theoretical Solution by Goudarzi et al.

For an isotropic incompressible filled elastomer with a Gaussian matrix, the effective stored-energy takes the following form:

$$\bar{\Psi}\left(\bar{I}_1, \bar{I}_2, c_p, c_i\right) = \frac{\bar{\mu}(c_p, c_i)}{2}\left[\bar{I}_1 - 3\right]$$

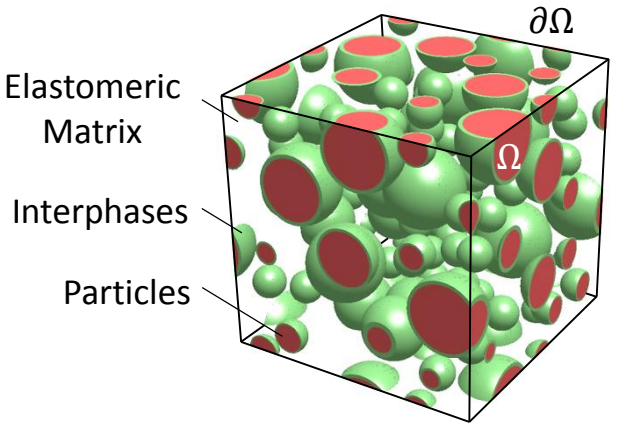

where $\bar{\mu}$ is defined implicitly through the expression:

$$\mathcal{F}_1\{\bar{\mu}, \mu_m\} \equiv \frac{c_i\left[q_4^2 - q_4(q_1+2q_2+q_3)+q_1q_3\right]+c_p\left[q_3(2q_1+q_2)-q_4(q_2+2q_3)\right]}{\sqrt{c_i^2(q_1+q_4)^2+2c_ic_p\left[q_4(2q_1+q_2)-q_1(q_2+2q_3)\right]+c_p^2(q_2^2-4q_1q_3)}} \times \left\{\tanh^{-1}\left[\frac{c_i(q_4-q_1)+c_pq_2+2\left(c_pq_3-c_iq_4\right)\frac{\bar{\mu}}{\mu_i}}{\sqrt{c_i^2(q_1+q_4)^2+2c_ic_p\left[q_4(2q_1+q_2)-q_1(q_2+2q_3)\right]+c_p^2(q_2^2-4q_1q_3)}}\right] - \tanh^{-1}\left[\frac{c_i(q_4-q_1)+c_pq_2+2\left(c_pq_3-c_iq_4\right)\frac{\mu_m}{\mu_i}}{\sqrt{c_i^2(q_1+q_4)^2+2c_ic_p\left[q_4(2q_1+q_2)-q_1(q_2+2q_3)\right]+c_p^2(q_2^2-4q_1q_3)}}\right]\right\} - \frac{1}{2}(q_3+q_4)\ln\left[\frac{c_i(\bar{\mu}-\mu_i)(\mu_iq_1+q_4\bar{\mu})-c_p\left(\mu_i^2q_1+\mu_1q_2\bar{\mu}+q_3\bar{\mu}^2\right)}{c_i(\mu_m-\mu_i)(\mu_iq_1+q_4\mu_m)-c_p\left(\mu_i^2q_1+\mu_1q_2\mu_m+q_3\mu_m^2\right)}\right] + \left(q_4 - \frac{c_p}{c_i}q_3\right)ln\left[\left(1-c_i-c_p\right)^{5/2}\frac{\bar{\mu}}{\mu_m}\right] = 0$$

with

$$q_1 = 38k^{10} + 225k^7 - 336k^5 + 200k^3 + 48$$

$$q_2 = 89k^{10} + 75k^7 - 168k^5 + 100k^3 - 96$$

$$q_3 = 48k^{10} - 300k^7 + 504k^5 - 300k^3 + 48$$

$$q_4 = \frac{4(k-1)^3(2k^3+3)(4k^6+16k^5+40k^4+55k^3+40k^2+16k+4)}{k^2+k+1}$$

$$k = 1 + \frac{t}{r} = \left(1 + \frac{c_i}{c_p}\right)^{1/3}$$

Goudarzi T, Spring DW, Paulino GH, Lopez-Pamies O, Filled elastomers: A theory of filler reinforcement based on hydrodynamic and interphasial effects. *Journal of the Mechanics and Physics of Solids*, Vol. 80, pp. 37-67, 2015

The Computed Effective Moduli Agree Well with Theory

We investigate the effective modulus of the composite, and compare our computational results with the theoretical solution.

Polydisperse

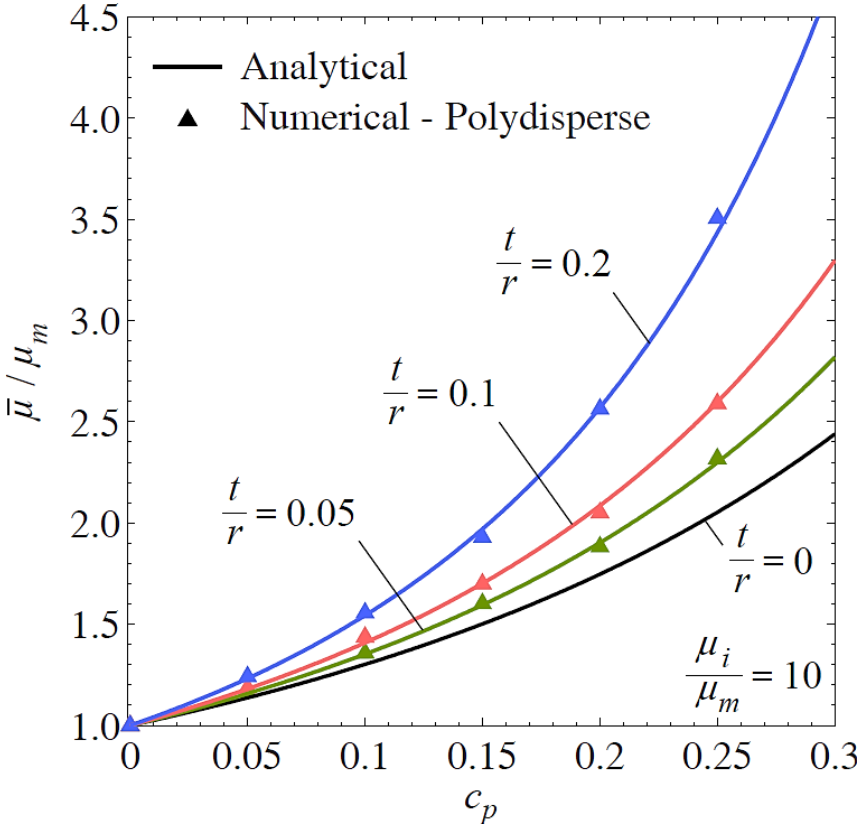

Monodisperse

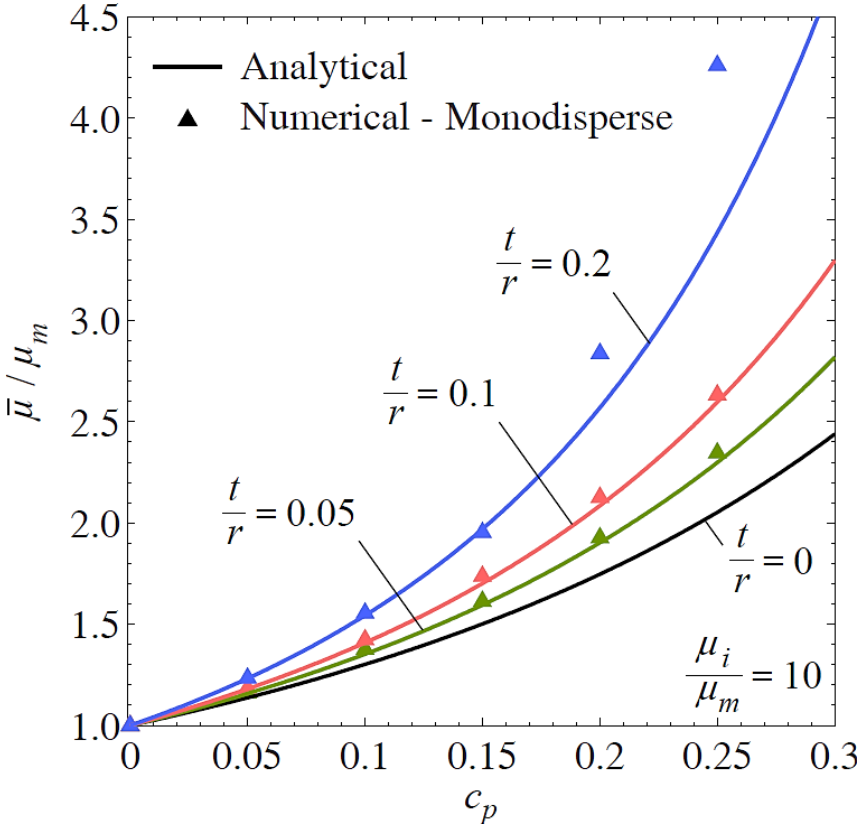

Goudarzi T, Spring DW, Paulino GH, Lopez-Pamies O, Filled elastomers: A theory of filler reinforcement based on hydrodynamic and interphasial effects. *Journal of the Mechanics and Physics of Solids*, Vol. 80, pp. 37-67, 2015

Interphases Provide an Explanation for the Wide Range of Experimentally Observed Effective Moduli

When we overlay the numerically computed effective moduli, we capture a wide range of the experimentally observed moduli.

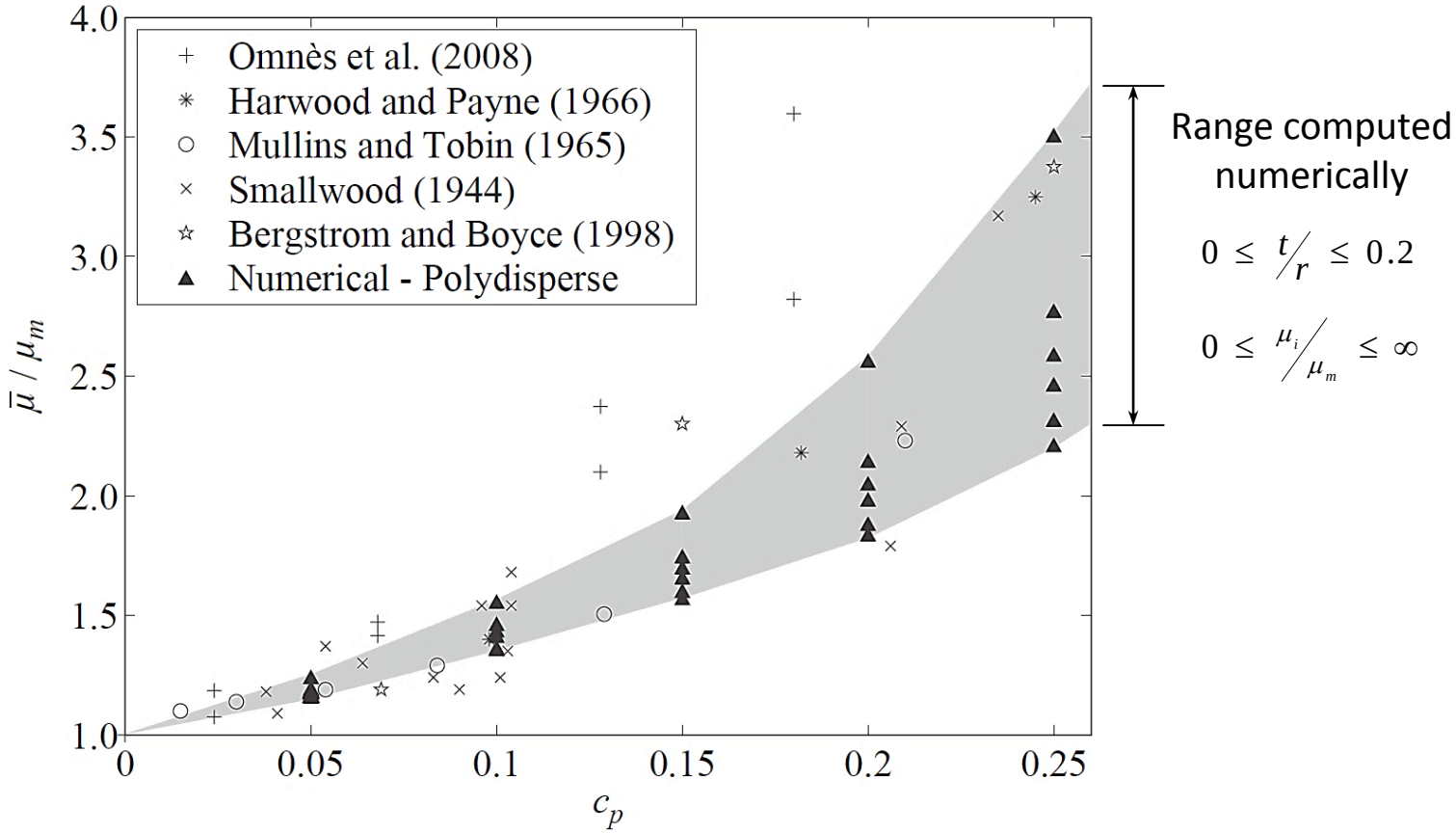

Daniel W. Spring. "Failure Processes in Soft and Quasi-Brittle Materials with Nonhomogeneous Microstructures." PhD Dissertation, Department of Civil and Environmental Engineering, UIUC, 2015.

Finite Deformation Response - Comparison with Theory

Comparison between theoretical and numerical results, $c_p = 0.15$.

Uniaxial Tension

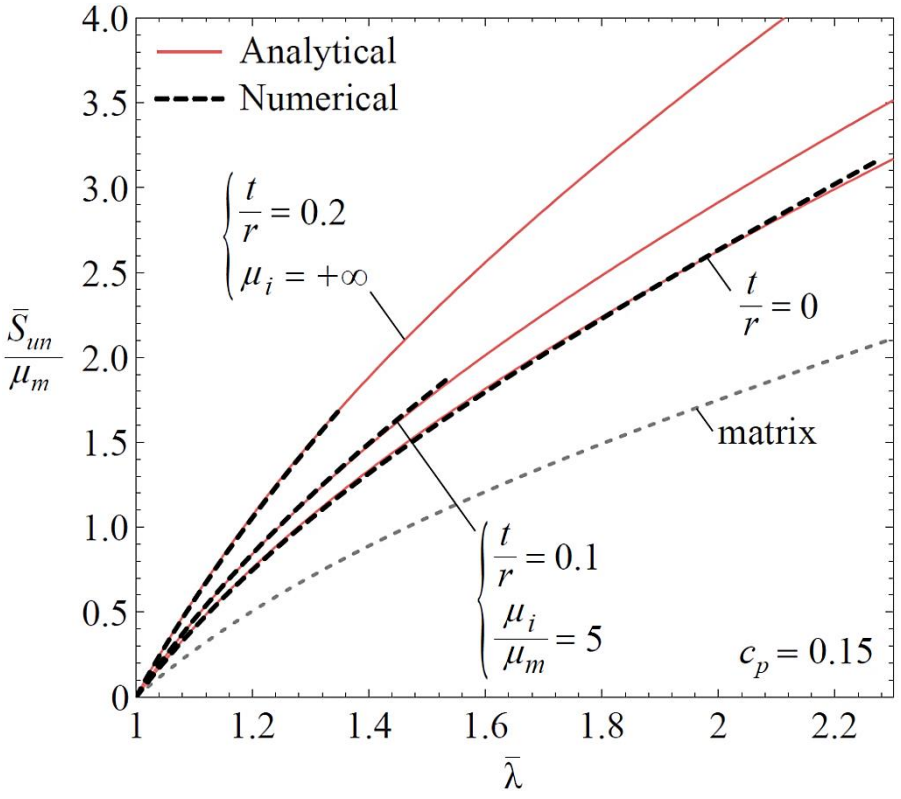

Simple Shear

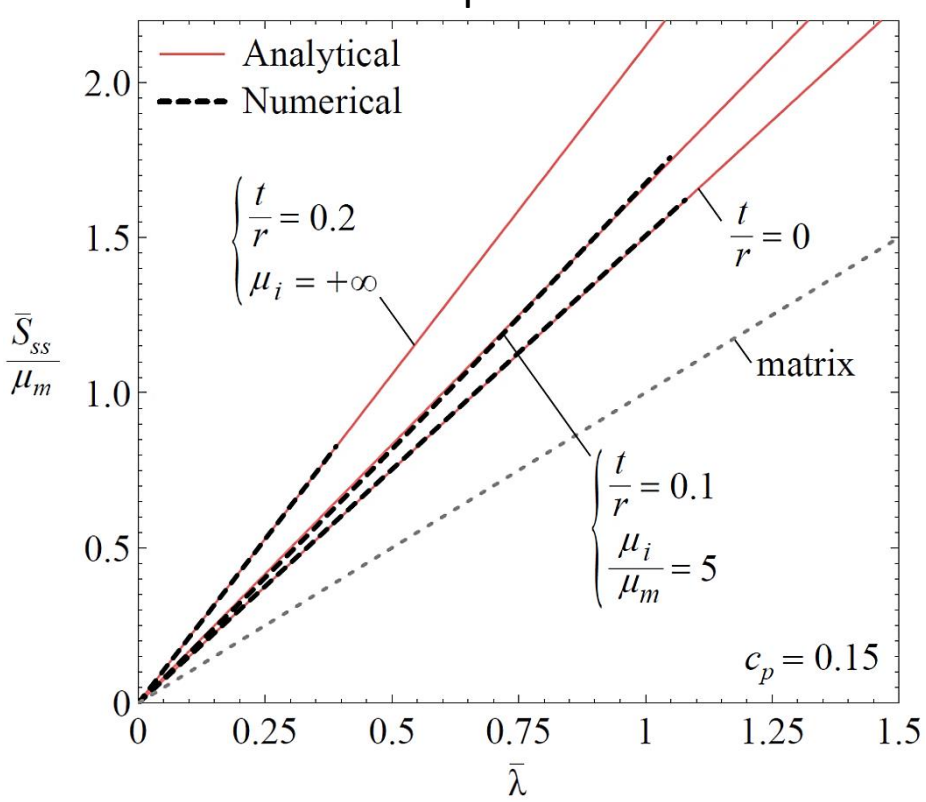

The presence of interphases has a comparable influence on the stiffness of the elastomer as does the presence of the particles alone.

Goudarzi T, Spring DW, Paulino GH, Lopez-Pamies O, Filled elastomers: A theory of filler reinforcement based on hydrodynamic and interphasial effects. *Journal of the Mechanics and Physics of Solids*, Vol. 80, pp. 37-67, 2015

Validation with FD Experimental Data from the Literature

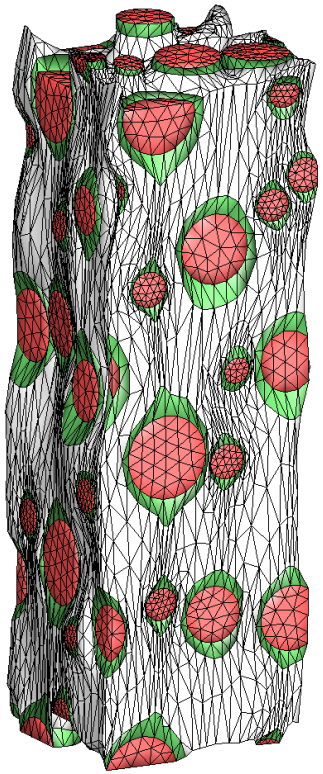

$c_p = 0.2085 \quad {}^{t}/_{r} = 0.2$

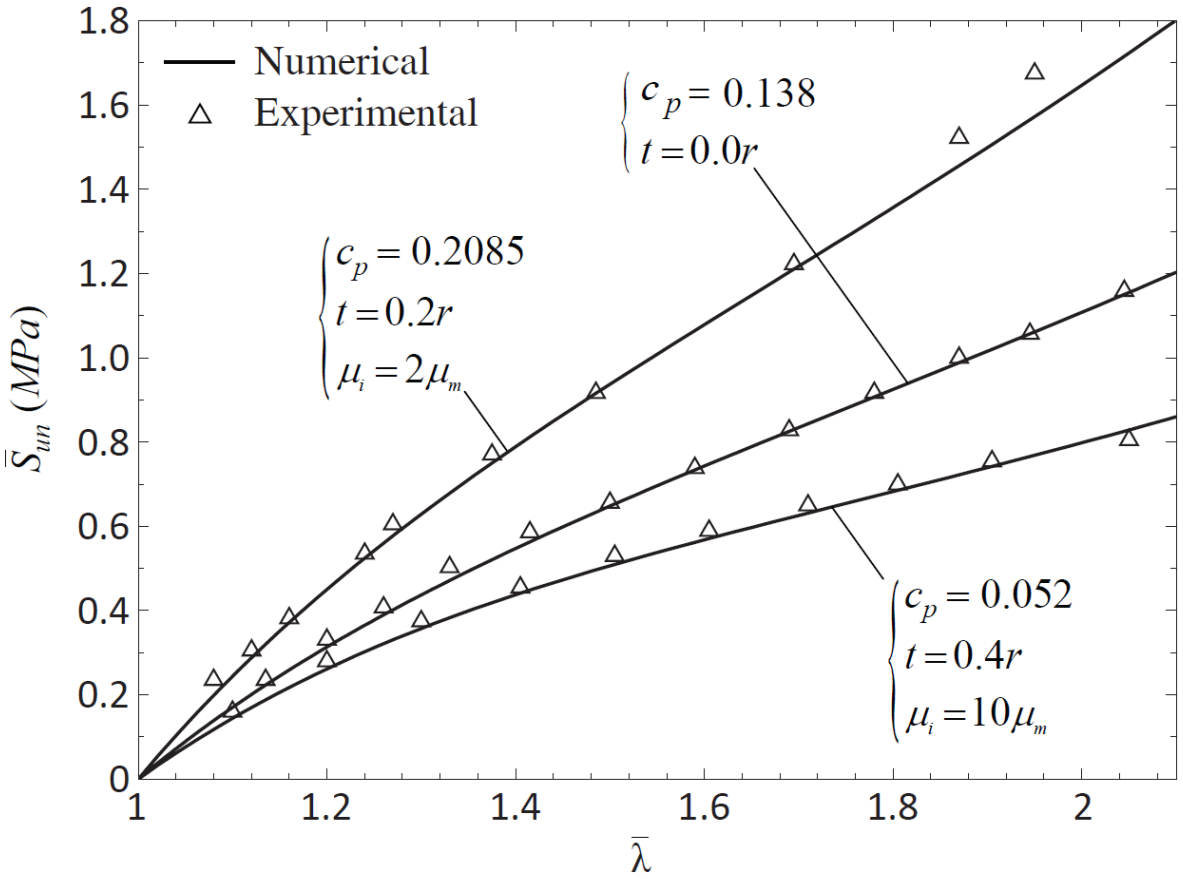

Mullins L, Tobin NR, 1965. Stress softening in rubber vulcanizates. Part I. Use of a strain amplification factor to describe the elastic behavior of filler-reinforced vulcanized rubber. Journal of Applied Polymer Science, Vol. 9, pp. 2993-3009

Jha V. "Carbon black filler reinforcement of elastomers." Ph.D. dissertation, Department of Materials, Queen Mary, University of London, 2008

Daniel W. Spring. "Failure Processes in Soft and Quasi-Brittle Materials with Nonhomogeneous Microstructures." PhD Dissertation, Department of Civil and Environmental Engineering, UIUC, 2015.

Presentation Structure

1. Perfectly Bonded Interphases in Particle Reinforced Elastomers

- Goudarzi T, **Spring DW**, Paulino GH, Lopez-Pamies O, Filled elastomers: A theory of filler reinforcement based on hydrodynamic and interphasial effects. *Journal of the Mechanics and Physics of Solids*, Vol. 80, pp. 37-67, 2015

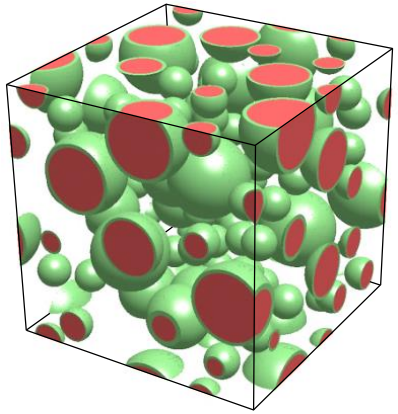

2. Interfacial Debonding in Particle Reinforced Elastomers

- **Spring DW**, Paulino GH, A growing library of three-dimensional cohesive elements for use in ABAQUS. *Engineering Fracture Mechanics*, Vol. 126, pp. 190-216, 2014.
- **Spring DW**, Paulino GH, Computational homogenization of the debonding of particle reinforced elastomers: The role of interphases in interfaces. *Under Review.*

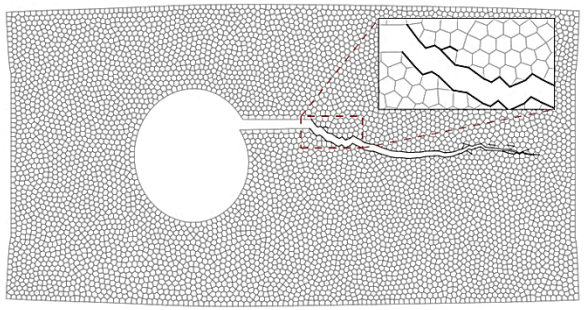

3. Reducing Mesh Bias in Dynamic Fracture Simulations Through Adaptive Operators

- Leon SE, **Spring DW**, Paulino GH, Reduction in mesh bias for dynamic fracture using adaptive splitting of polygonal finite elements. *International Journal for Numerical Methods in Engineering*, Vol. 100, pp. 555-576, 2014.
- **Spring DW**, Leon SE, Paulino GH, Unstructured polygonal meshes with adaptive refinement for the numerical simulation of dynamic cohesive fracture. *International Journal of Fracture*, Vol. 189, pp. 33-57, 2014.

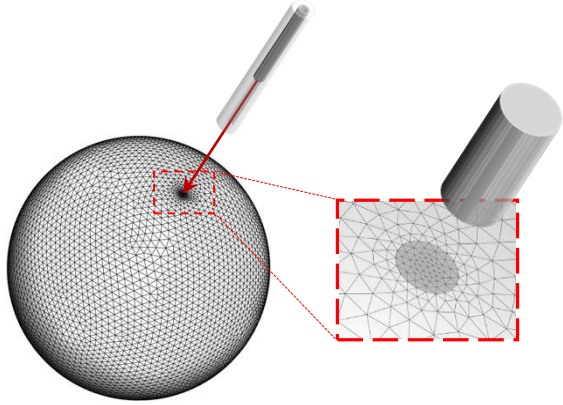

4. Regularizing Pervasive Fracture and Fragmentation Behavior in Three-Dimensions

- **Spring DW**, Paulino GH, Numerical unstructuring as a means for achieving pervasive fracture and fragmentation in three-dimensions. *In Preparation*.

Interfacial Failure Occurs Under Large Applied Strains

Several experimental investigations have shown the clear localization of damage (interfacial debonding) around stiff inclusions, at large strains.

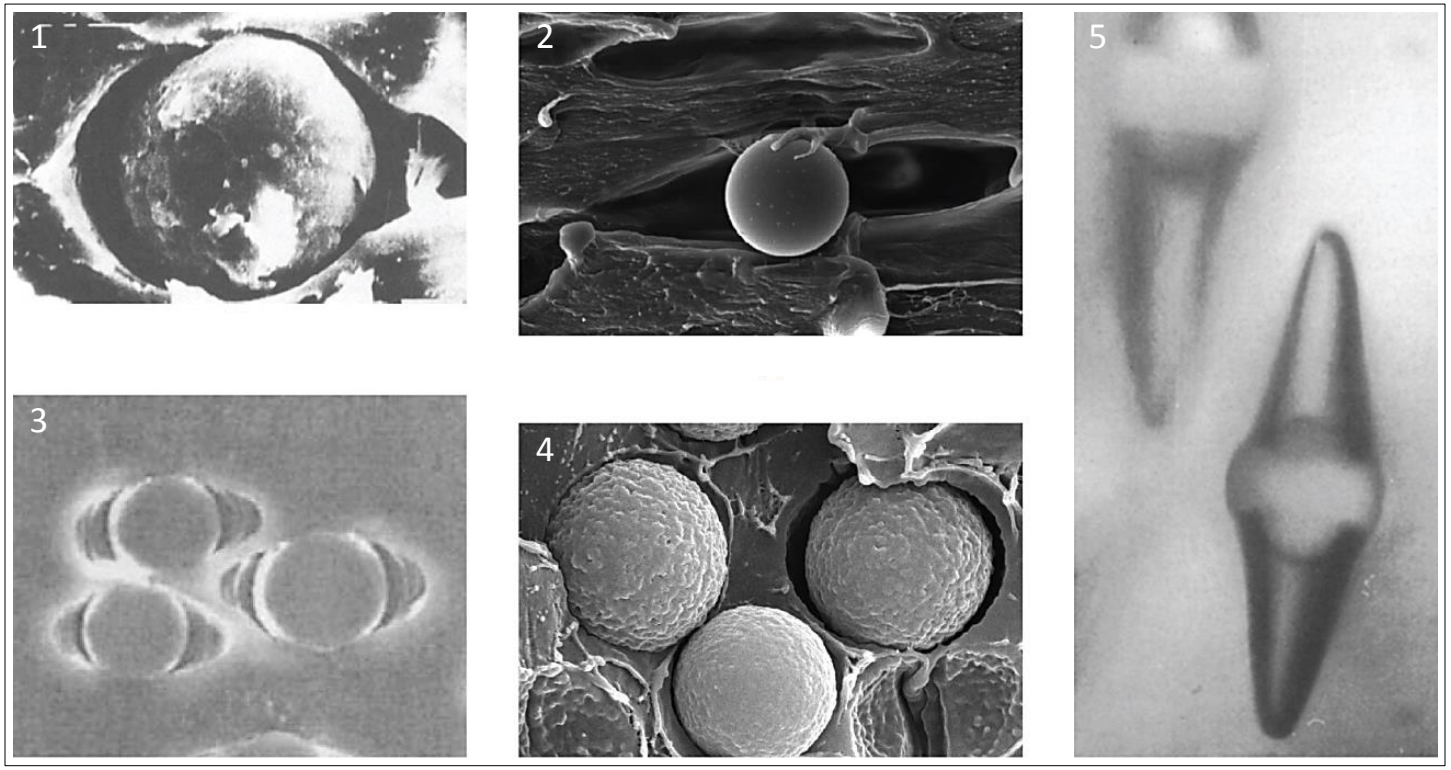

[1]Lahiri J, Paul A, Effect of interface on the mechanical behavior of glass bead-filled PVC. *Journal of Materials Science*, Vol. 20, pp. 2253–2259, 1985.

[2]Bai S-L , Chen J, Huang Z, Yu Z, The role of the interfacial strength in glass bead filled HDPE. *Journal of Materials Science Letters*, Vol. 19, pp. 1587–1589, 2000.

[3]Thio YS, Argon AS, Cohen RE, Role of interfacial adhesion strength on toughening polypropylene with rigid particles. *Polymer*, Vol. 45, pp. 3139–3147, 2004.

[4]Renner K, Micromechanical deformation process in polymer composites, Ph.D. thesis, Budapest University of Technology and Economics, 2010.

[5]Zhuk AV, Knunyants NN, Oshmyan VG, Topolkaraev VA, Berlin AA, Debonding microprocesses and interfacial strength in particle-filled polymer materials. *Journal of Materials* Science, Vol. 28, pp. 4595–4606, 1993.

Cohesive Elements Account for Interfacial Debonding

Intrinsic cohesive elements are inserted between each particle and its corresponding interphase to account for interfacial debonding.

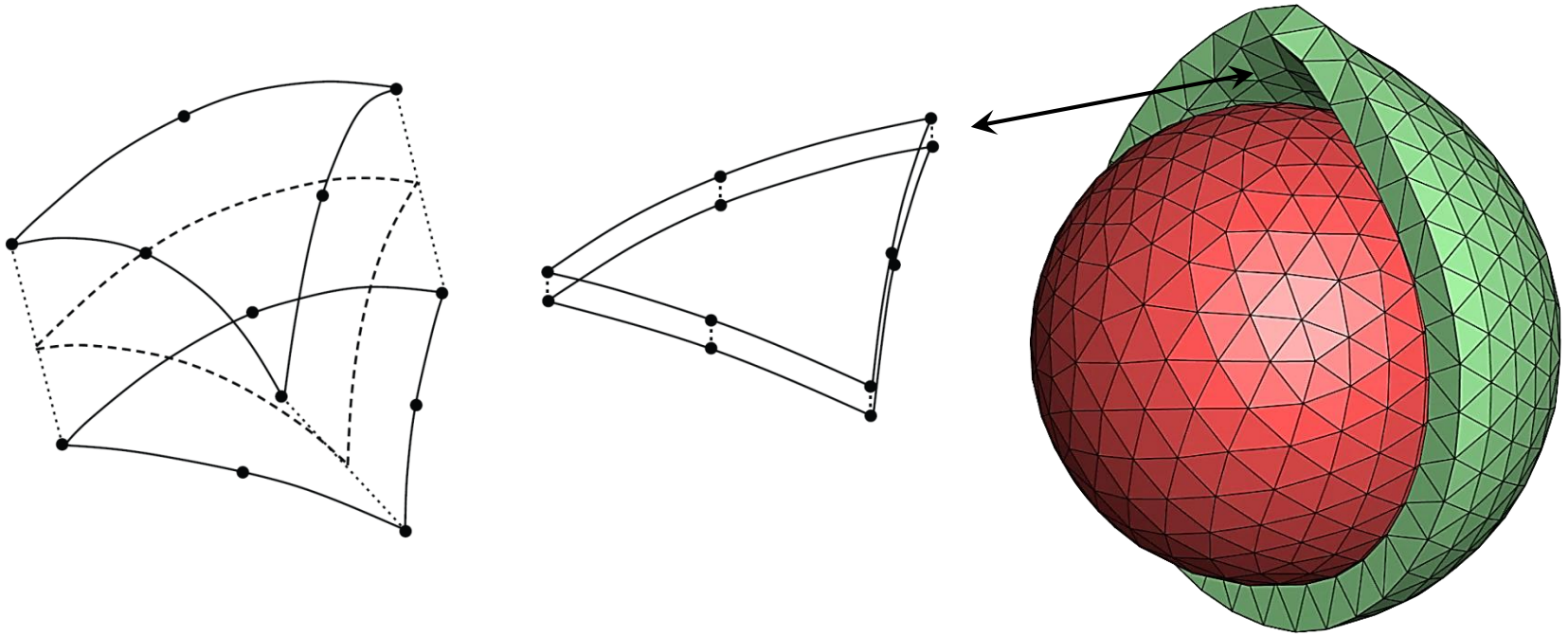

- The cohesive elements have zero thickness and, upon separation, impart a traction to the adjacent bulk elements
- The cohesive elements are implemented as a user supplied subroutine in a commercial finite element analysis software package

Spring DW, Paulino GH, A growing library of three-dimensional cohesive elements for use in ABAQUS. *Engineering Fracture Mechanics*, Vol. 126, pp. 190-216, 2014.

Park-Paulino-Roesler (PPR) Potential-Based Cohesive Model

The cohesive model is defined by a potential function

$$\boldsymbol{\Psi}(\Delta_n,\Delta_t)=\min(\phi_n,\phi_t)+\left[\Gamma_n\left(1-\frac{\Delta_n}{\delta_n}\right)^{\alpha}\left(\frac{m}{\alpha}+\frac{\Delta_n}{\delta_n}\right)^{m}+\langle\phi_n-\phi_t\rangle\right]\times\left[\Gamma_t\left(1-\frac{|\Delta_t|}{\delta_t}\right)^{\beta}\left(\frac{n}{\beta}+|\Delta_t|\delta_t\right)^{n}+\langle\phi_t-\phi_n\rangle\right]$$

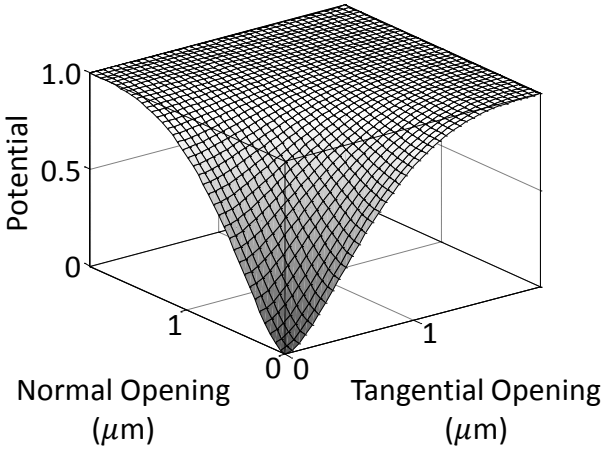

User inputs:

ϕ_n, ϕ_t	(Fracture energy)
σ_n, τ_t	(Cohesive strength)
α, β	(Softening shape parameter)
λ_n, λ_t	(Initial slope indicator)

From the cohesive potential, one can determine the traction-separation relations by taking the respective derivatives.

$$T_n(\Delta_n,\Delta_t)=\frac{\partial\boldsymbol{\Psi}}{\partial\Delta_n},$$

$$T_t(\Delta_n,\Delta_t)=\frac{\partial\boldsymbol{\Psi}}{\partial\Delta_t},$$

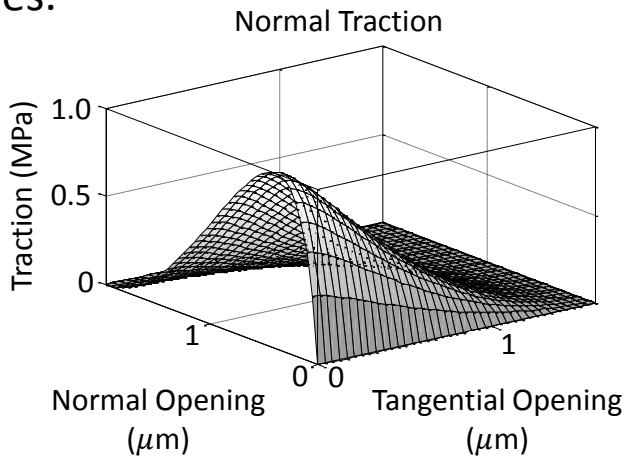

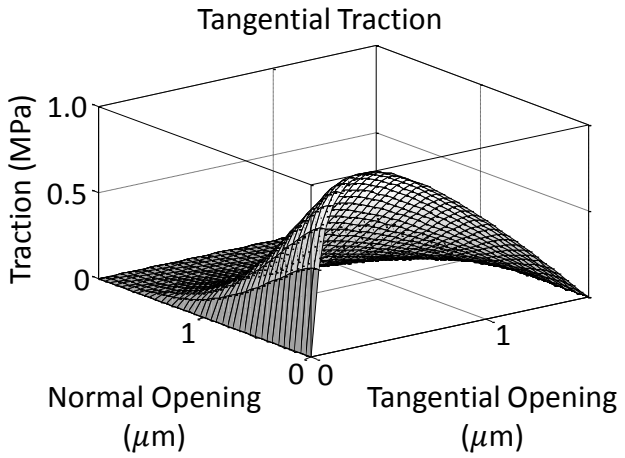

Park K, Paulino GH, Roesler JR, 2009. A unified potential-based cohesive model for mixed-mode fracture. *Journal of the Mechanics and Physics of Solids*. Vol. 57, No. 6, pp. 891-908.

A New Coupled Cohesive-Friction Model

To account for friction at the interface, we developed a new coupled cohesive-friction model. The contribution of friction to the tangential force is defined as:

$$\mathbf{T} = \begin{Bmatrix} T_n \\ T_t \frac{\Delta_2}{\Delta_t} + T_F \left(\frac{|\Delta_2|}{\Delta_t}\right) \frac{\dot{\mathbf{\Delta}}_2}{|\dot{\mathbf{\Delta}}_2|} \\ T_t \frac{\Delta_3}{\Delta_t} + T_F \left(\frac{|\Delta_3|}{\Delta_t}\right) \frac{\dot{\mathbf{\Delta}}_3}{|\dot{\mathbf{\Delta}}_3|} \end{Bmatrix}$$

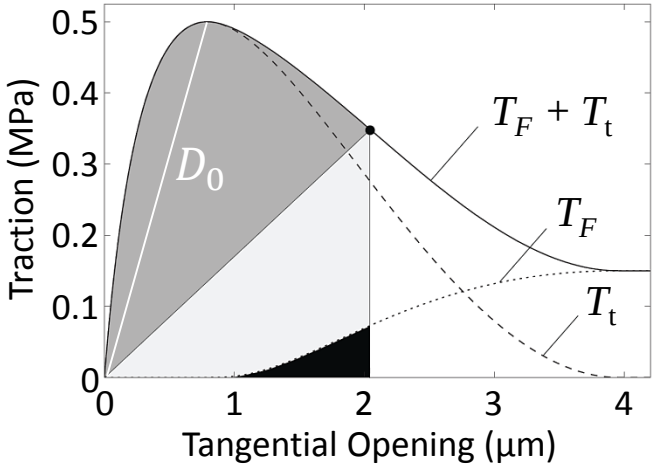

The above contribution is general. However, we derived a new friction model to be coupled specifically to the PPR cohesive model, and to adjust as the cohesive model adjusts:

$$T_F = \mu\kappa(\Delta_t)|T_n|, \qquad \kappa(\Delta_t) = \left(1 - \frac{T_t(0,\Delta_t)}{D_0\Delta_t}\right)^s \qquad \text{if } T_n < 0 \text{ and } \Delta_t > \lambda_t\delta_t$$

where:

$$D_0 = \frac{\Gamma_t}{\delta_t}\left[n(1-\lambda_t)^\beta\left(\frac{n}{\beta}+\lambda_t\right)^{n-1} - \beta(1-\lambda_t)^{\beta-1}\left(\frac{n}{\beta}+\lambda_t\right)^n\right]\left[\Gamma_n\left(\frac{m}{\alpha}\right)^m + \langle\phi_n - \phi_t\rangle\right]\frac{1}{\lambda_t\delta_t}$$

Spring DW, Paulino GH, Computational homogenization of the debonding of particle reinforced elastomers: The role of interphases in interfaces. *Under Review.*

Decomposition of the Coupled Cohesive-Friction Model

- Cohesive Forces

$$\mathbf{T} = \begin{Bmatrix} T_n \\ T_t \frac{\Delta_2}{\Delta_t} + T_F \left(\frac{|\Delta_2|}{\Delta_t}\right) \frac{\dot{\mathbf{\Delta}}_2}{|\dot{\mathbf{\Delta}}_2|} \\ T_t \frac{\Delta_3}{\Delta_t} + T_F \left(\frac{|\Delta_3|}{\Delta_t}\right) \frac{\dot{\mathbf{\Delta}}_3}{|\dot{\mathbf{\Delta}}_3|} \end{Bmatrix}$$

- Friction Forces

$$\mathbf{T} = \begin{Bmatrix} T_n \\ T_t \frac{\Delta_2}{\Delta_t} + T_F \left(\frac{|\Delta_2|}{\Delta_t}\right) \frac{\dot{\mathbf{\Delta}}_2}{|\dot{\mathbf{\Delta}}_2|} \\ T_t \frac{\Delta_3}{\Delta_t} + T_F \left(\frac{|\Delta_3|}{\Delta_t}\right) \frac{\dot{\mathbf{\Delta}}_3}{|\dot{\mathbf{\Delta}}_3|} \end{Bmatrix}$$

- Coupled Forces

$$\mathbf{T} = \begin{Bmatrix} T_n \\ T_t \frac{\Delta_2}{\Delta_t} + T_F \left(\frac{|\Delta_2|}{\Delta_t}\right) \frac{\dot{\mathbf{\Delta}}_2}{|\dot{\mathbf{\Delta}}_2|} \\ T_t \frac{\Delta_3}{\Delta_t} + T_F \left(\frac{|\Delta_3|}{\Delta_t}\right) \frac{\dot{\mathbf{\Delta}}_3}{|\dot{\mathbf{\Delta}}_3|} \end{Bmatrix}$$

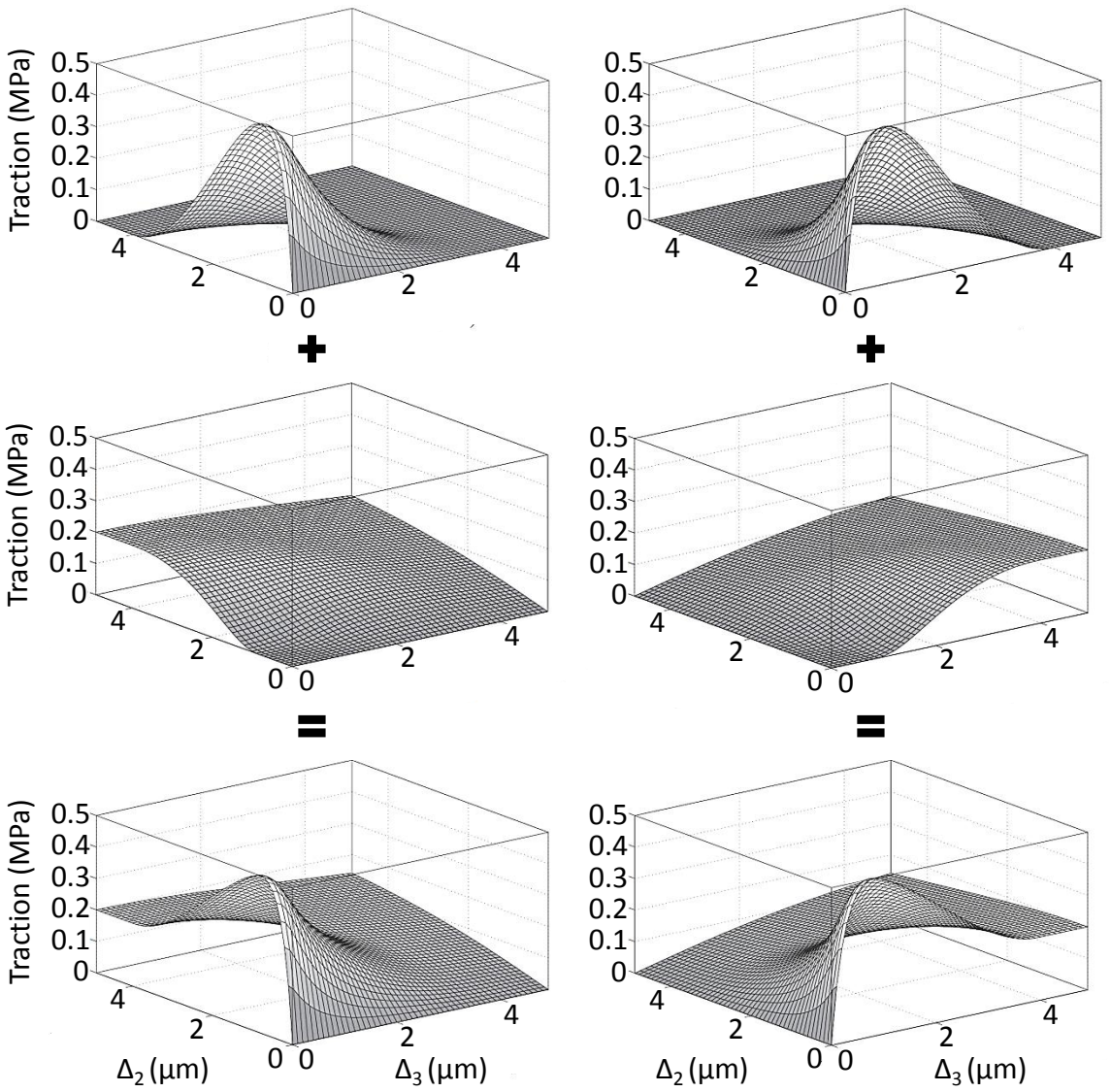

Spring DW, Paulino GH, Computational homogenization of the debonding of particle reinforced elastomers: The role of interphases in interfaces. *Under Review.*

Influence of Friction on the Global Response

Frictional forces contribute little to the macroscopic constitutive response of the composite.

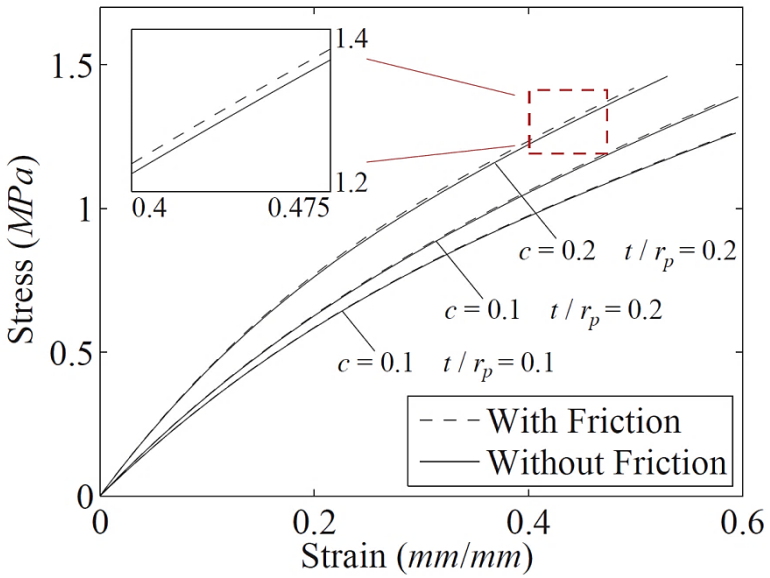

Deformed Geometry

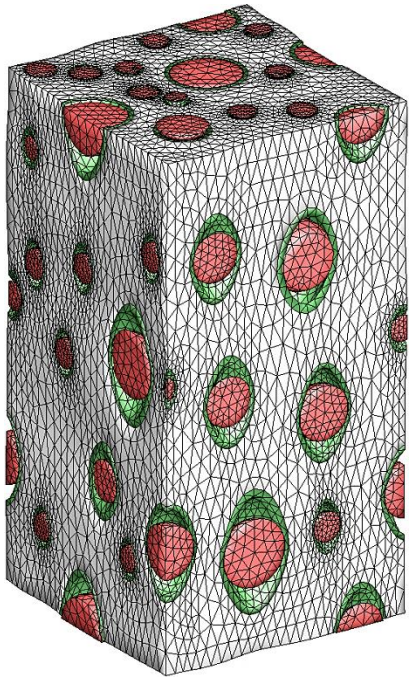

Stress Field

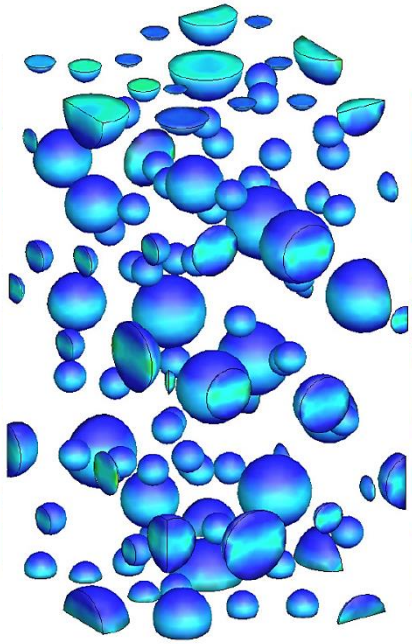

$c_p = 0.10 \qquad {}^{t}/_{r} = 0.2 \qquad \mu_i = 10 \times \mu_m = 10.0MPa$

Previous investigations have neglected the influence of friction. We verify this assumption in uniaxial tension.

Spring DW, Paulino GH, Computational homogenization of the debonding of particle reinforced elastomers: The role of interphases in interfaces. *Under Review.*

Matouš K, Geubelle, PH, Multiscale modelling of particle debonding in reinforced elastomers subjected to finite deformations. *International Journal for Numerical Methods in Engineering*. Vol. 65, pp. 190-223, 2006.

Experimental Validation with Interfacial Debonding

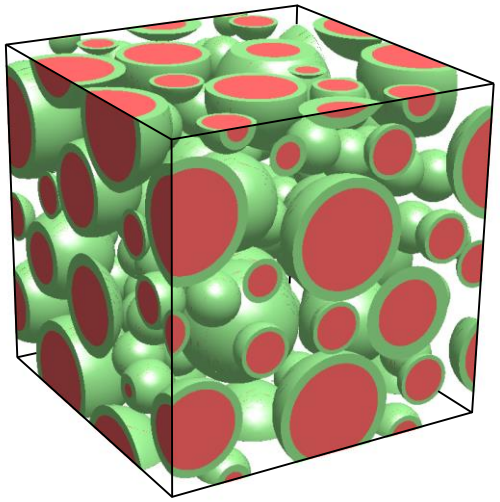

$c_p = 0.26$ $\quad t/r = 0.2$

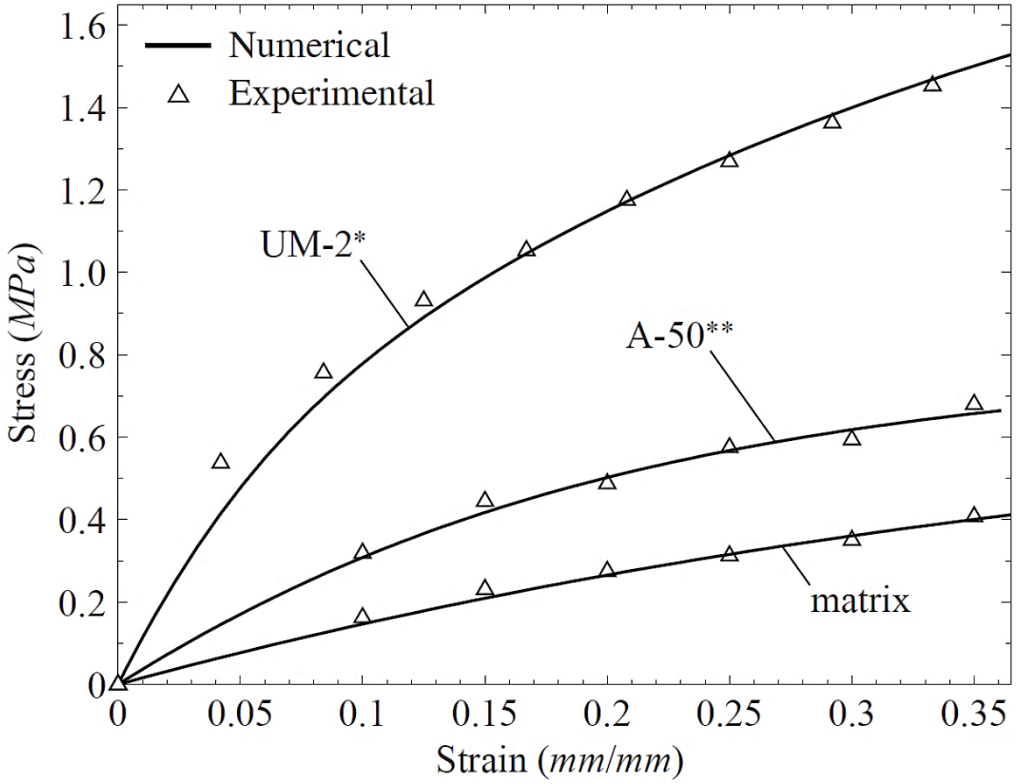

Matrix: $\mu_m = 0.54MPa$

UM-2: $\mu_m = 0.54MPa$
$\mu_i = 3 \times \mu_m = 1.62MPa$

A-50: $\mu_m = 2.1MPa$
$\mu_i = 2 \times \mu_m = 4.2MPa$

Cohesive: $\phi = 1.0N/m \quad \sigma_{\max} = 0.5MPa$

$$\Psi\left(I_1\right) = \frac{3^{1-\alpha}}{2\alpha}\mu_m\left[I_1^{\alpha} - 3^{\alpha}\right] \quad \text{if} \quad J = 1$$

where $\alpha = 0.2$

*Suzuki N, Ito M, Yatsuyanagi F, Effect of rubber filler interactions on deformation behavior of silica filled SBR systems. *Polymer*. Vol. 46, pp. 193-201, 2005.

**Yatsuyanagi F, Suzuki N, Ito M, Kaidou H, Effect of surface chemistry of silica particles on the mechanical properties of silica filled Styrene-Butadiene rubber systems. *Polymer Journal*. Vol. 34, pp. 332-339, 2002.

Lopez-Pamies O, A new I_1-based hyperelastic model for rubber elastic materials. *Comptes Rendus Mecanique* Vol. 38, pp. 3–11, 2010.

Remarks

- The presence of interphases has a comparable influence on the stiffness of the elastomer as does the presence of the particles alone.
- The presence of interphases and interfacial debonding explains the wide range of experimentally observed deviations in behavior in particle reinforced composites.
- The overall stiffness of the composite is more sensitive to the interphase thickness than to the interphase modulus.
- Interfacial debonding can be included through the use of cohesive elements.
- Frictional effects are negligible in tension induced debonding.
- Recognizing the role and main factors influencing interfacial adhesion and proper surface modification may lead to significant progress in many fields of research and development, as well as related technologies.

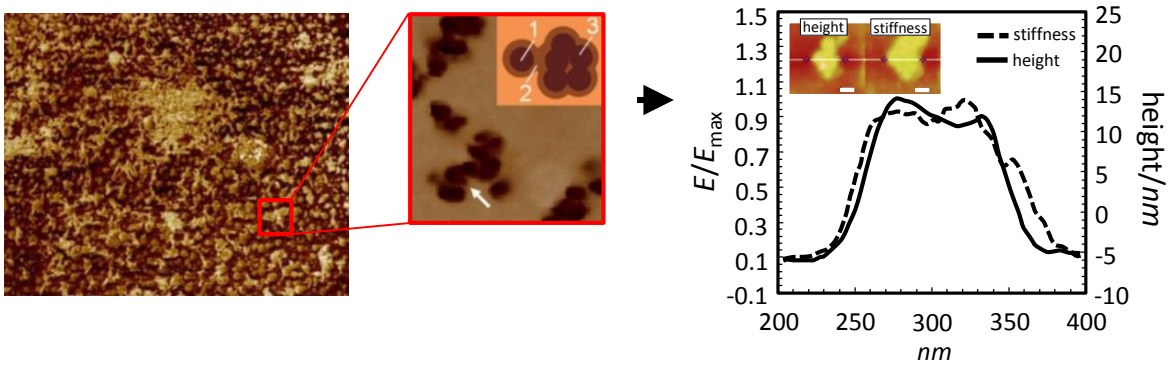

Goudarzi T, Spring DW, Paulino GH, Lopez-Pamies O, Filled elastomers: A theory of filler reinforcement based on hydrodynamic and interphasial effects. *Journal of the Mechanics and Physics of Solids*, Vol. 80, pp. 37-67, 2015.

Spring DW, Paulino GH, A growing library of three-dimensional cohesive elements for use in ABAQUS. *Engineering Fracture Mechanics*, Vol. 126, pp. 190-216, 2014.

Spring DW, Paulino GH, Computational homogenization of the debonding of particle reinforced elastomers: The role of interphases in interfaces. *Under Review.*

Presentation Structure

1. Perfectly Bonded Interphases in Particle Reinforced Elastomers

- Goudarzi T, **Spring DW**, Paulino GH, Lopez-Pamies O, Filled elastomers: A theory of filler reinforcement based on hydrodynamic and interphasial effects. *Journal of the Mechanics and Physics of Solids*, Vol. 80, pp. 37-67, 2015

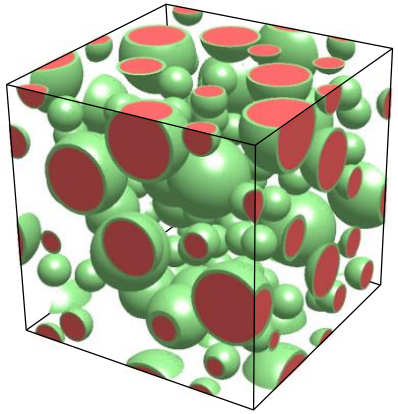

2. Interfacial Debonding in Particle Reinforced Elastomers

- **Spring DW**, Paulino GH, A growing library of three-dimensional cohesive elements for use in ABAQUS. *Engineering Fracture Mechanics*, Vol. 126, pp. 190-216, 2014.
- **Spring DW**, Paulino GH, Computational homogenization of the debonding of particle reinforced elastomers: The role of interphases in interfaces. *Under Review.*

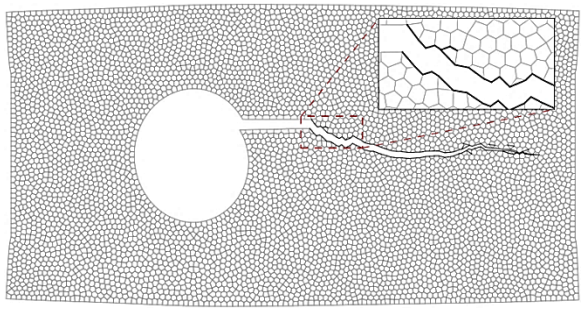

3. Reducing Mesh Bias in Dynamic Fracture Simulations Through Adaptive Operators

- Leon SE, **Spring DW**, Paulino GH, Reduction in mesh bias for dynamic fracture using adaptive splitting of polygonal finite elements. *International Journal for Numerical Methods in Engineering*, Vol. 100, pp. 555-576, 2014.
- **Spring DW**, Leon SE, Paulino GH, Unstructured polygonal meshes with adaptive refinement for the numerical simulation of dynamic cohesive fracture. *International Journal of Fracture*, Vol. 189, pp. 33-57, 2014.

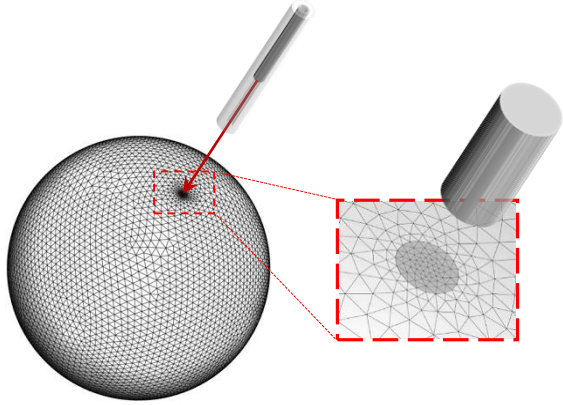

4. Regularizing Pervasive Fracture and Fragmentation Behavior in Three-Dimensions

- **Spring DW**, Paulino GH, Numerical unstructuring as a means for achieving pervasive fracture and fragmentation in three-dimensions. *In Preparation*.

Dynamic Material Failure is Commonplace in Engineering

Examples of dynamic failure in an engineering application:

Seismic Design

usgs.gov

Oil & Gas Extraction

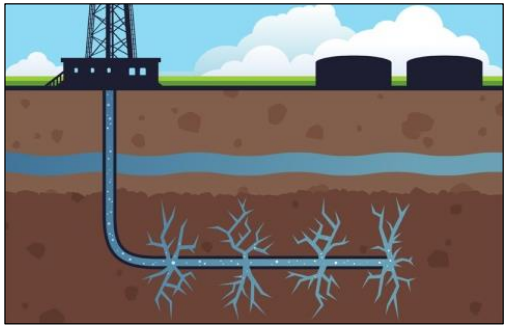

mlive.com

Renewable Energy

telegraph.co.uk

There is a wide spectrum of failure behavior:

Single/Dominant Cracks

swanston.com

Crack Branching ↔ Crack Coalescence

Range of fracture behavior

Pervasive Cracking and Fragmentation

wellcoll.nl

Dynamic Fracture Code - Overview

The code is implemented in C, and uses the TopS data structure to handle the background data management.

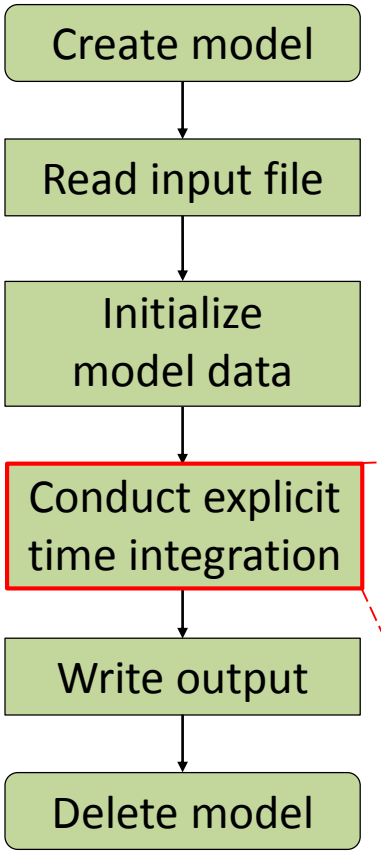

Bulk Elements (Continuum Behavior) | Dynamically Inserted Cohesive Elements

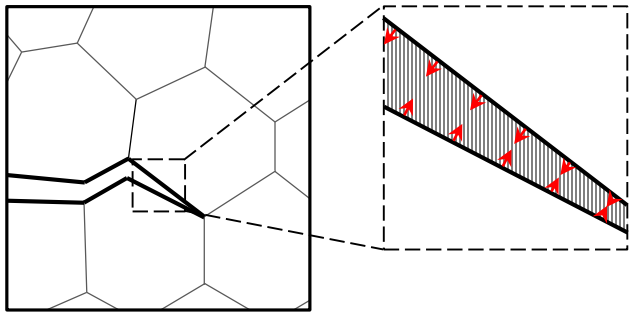

Traction-Separation Relation

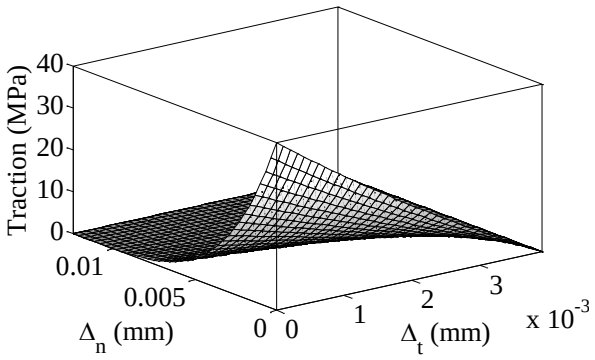

Explicit time integration for the extrinsic fracture code

Initialization: displacements ($\mathbf{u}_0$), velocity ($\dot{\mathbf{u}}_0$), acceleration ($\ddot{\mathbf{u}}_0$)
for $n = 0$ to n_{max} do
  Update displacement: $\mathbf{u}_{n+1} = \mathbf{u}_n + \Delta t \dot{\mathbf{u}}_n + \Delta t^2/2 \ddot{\mathbf{u}}_n$
  Check the insertion of cohesive elements
  Update acceleration: $\ddot{\mathbf{u}}_{n+1} = \mathbf{M}^{-1}\left(\mathbf{R}^{\text{ext}}_{n+1} + \mathbf{R}^{\text{coh}}_{n+1} - \mathbf{R}^{\text{int}}_{n+1}\right)$
  Update velocity: $\dot{\mathbf{u}}_{n+1} = \dot{\mathbf{u}}_n + \Delta t/2(\ddot{\mathbf{u}}_n + \ddot{\mathbf{u}}_{n+1})$
  Update boundary conditions
end for

Celes W, Paulino GH, Espinha R, A compact adjacency-based topological data structure for finite element mesh representation. *International Journal for Numerical Methods in Engineering*, vol. 64, pp. 1529-1556, 2005.

Unstructured Meshes for Dynamic Cohesive Fracture

One of the primary critiques of the cohesive element method is its mesh dependency.

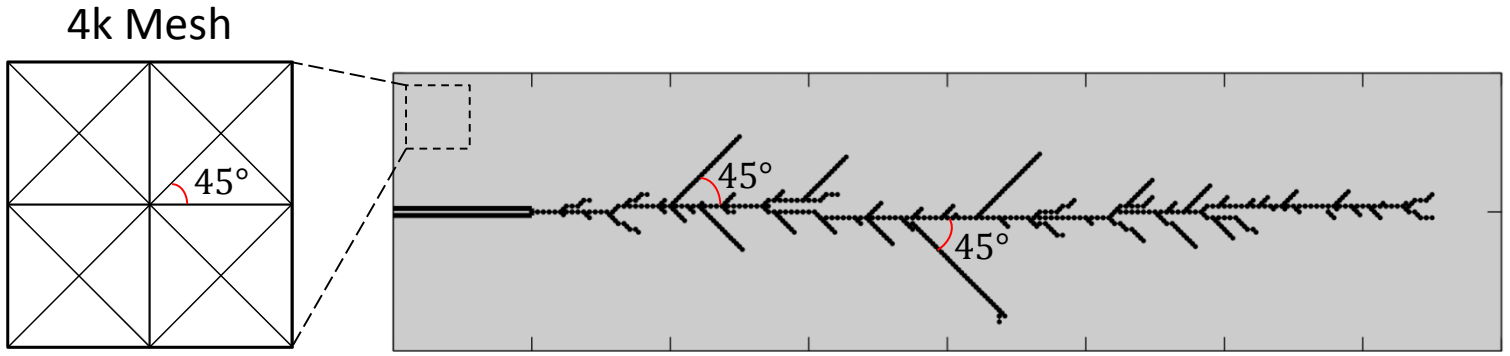

Structured meshes may artificially bias fracture behavior, presenting preferred paths for cracks to propagate along.

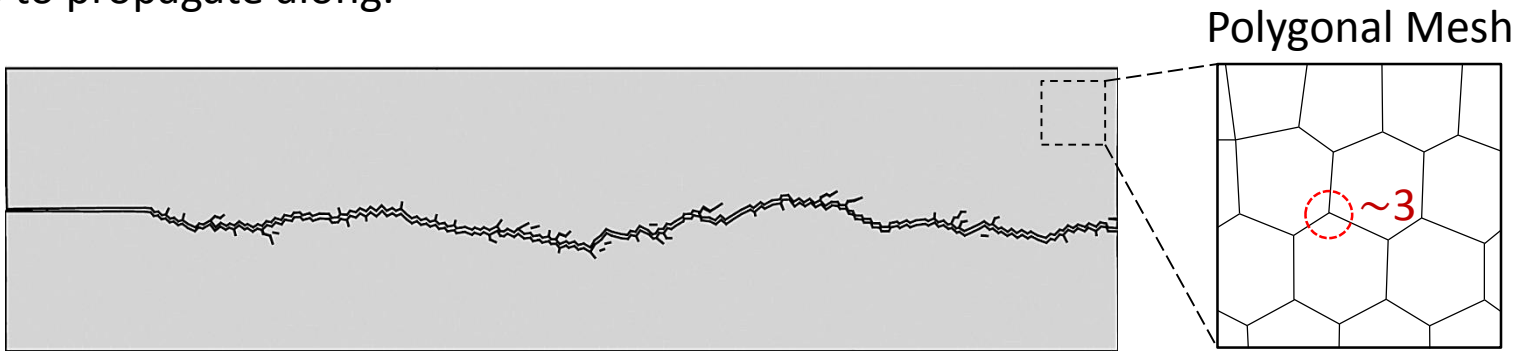

Polygonal meshes are isotropic, but have a limited number of crack paths at each node.

Zhang Z, Paulino GH, Celes W, 2007. Extrinsic cohesive zone modeling of dynamic fracture and microbranching instability in brittle materials. *International Journal for Numerical Methods in Engineering*. vol. 72, pp. 893-923.

Spring DW, Leon SE, Paulino GH, Unstructured polygonal meshes with adaptive refinement for the numerical simulation of dynamic cohesive fracture. *International Journal of Fracture*, Vol. 189, pp. 33-57, 2014.

How to Quantify Mesh Isotropy/Anisotropy (Mesh Bias)

Dijkstra's algorithm is used to compute the shortest path between two points in the mesh.

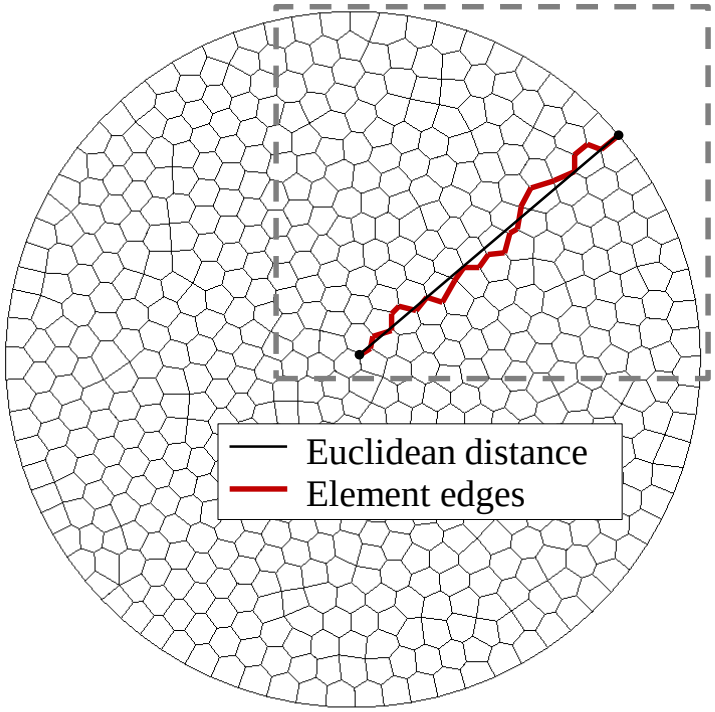

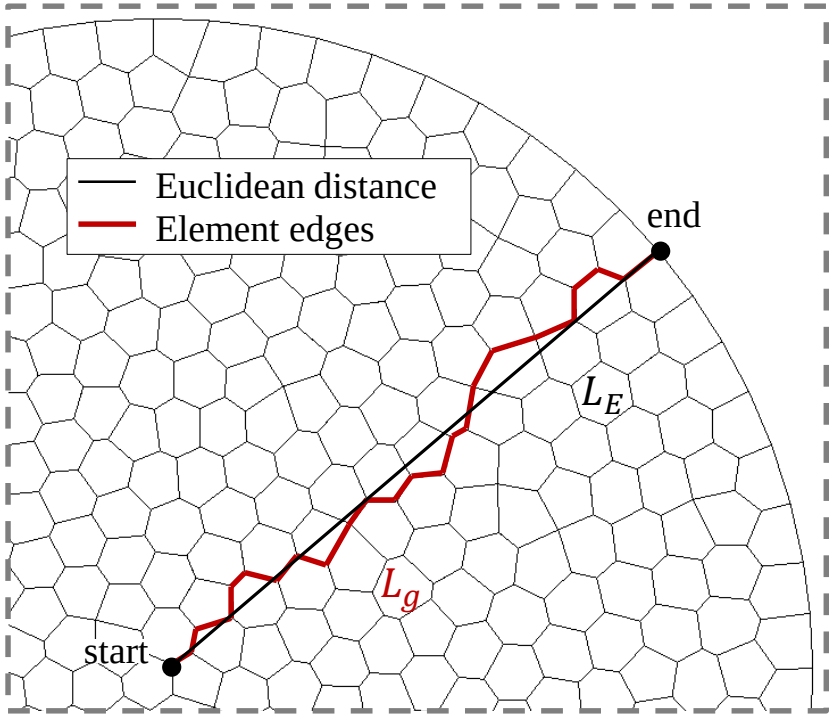

The path deviation is computed as:

$$\eta = \frac{L_g}{L_E} - 1$$

Dijkstra EW, A note on two problems in connexion with graphs. *Numerische Mathematik*. Vol. 1, pp. 269–227, 1959.

Rimoli JJ, Rojas JJ, Meshing strategies for the alleviation of mesh-induced effects in cohesive element models. International Journal of Fracture, DOI:10.1007/s10704-015-0013-6

Spring DW, Leon SE, Paulino GH, Unstructured polygonal meshes with adaptive refinement for the numerical simulation of dynamic cohesive fracture. *International Journal of Fracture*, Vol. 189, pp. 33-57, 2014.

Quantifying Mesh Isotropy/Anisotropy

A study was conducted on the path deviation over a range of 180°

$$\eta = \frac{L_g}{L_E} - 1$$

4k Mesh

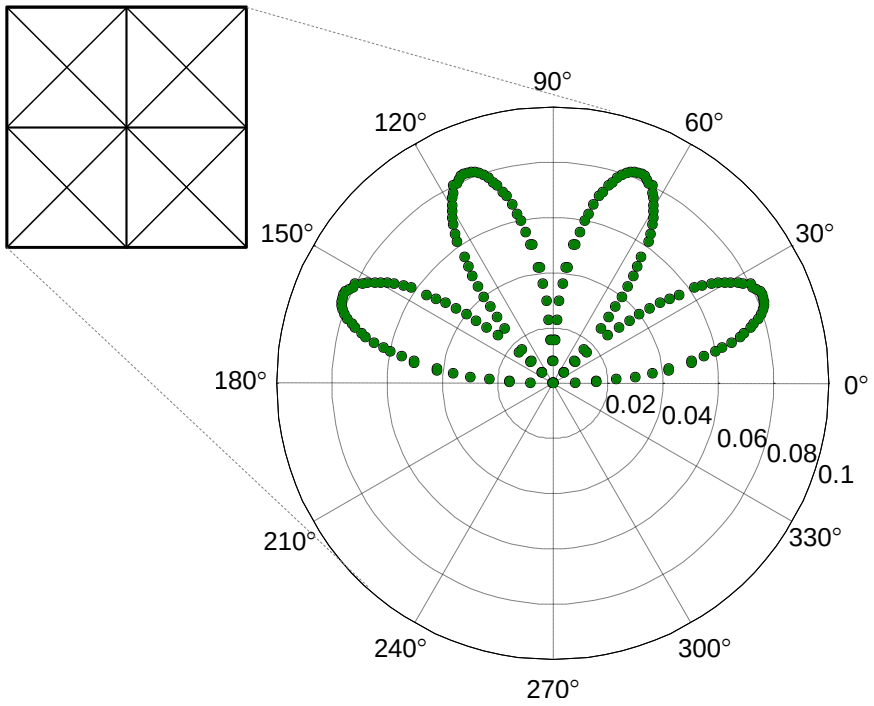

Polygonal Mesh

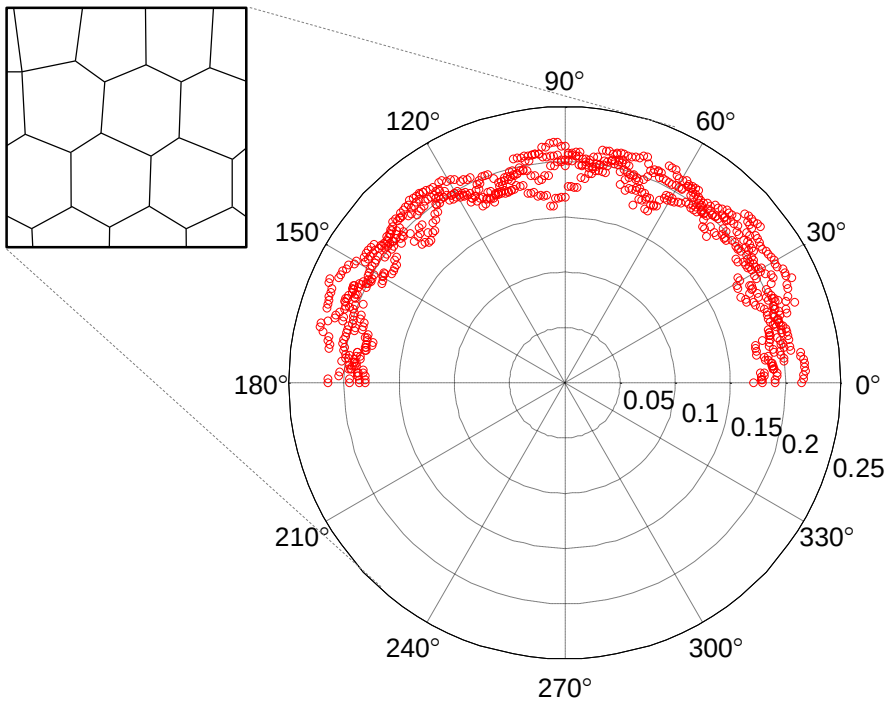

The structured 4k mesh is anisotropic, while the unstructured polygonal discretization is isotropic. However, the path deviation in the polygonal mesh is significantly higher that that in the structured mesh.

Rimoli JJ, Rojas JJ, Meshing strategies for the alleviation of mesh-induced effects in cohesive element models. International Journal of Fracture, DOI:10.1007/s10704-015-0013-6

Leon SE*, Spring DW*, Paulino GH, Reduction in mesh bias for dynamic fracture using adaptive splitting of polygonal finite elements. *International Journal for Numerical Methods in Engineering*, Vol. 100, pp. 555-576, 2014.

Element-Splitting Operator for Reducing Mesh Bias

In order to reduce the path deviation in the unstructured polygonal mesh, we propose using an **element-splitting** topological operator to increase the number of fracture paths at each node in the mesh.

We restrict elements to be split along the path which minimizes the difference between the areas of the resulting split elements.

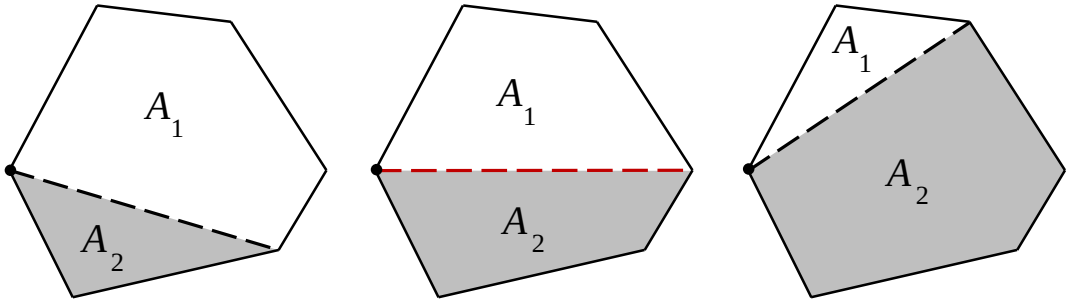

The propagating crack now has twice as many paths on which it could travel at each node.

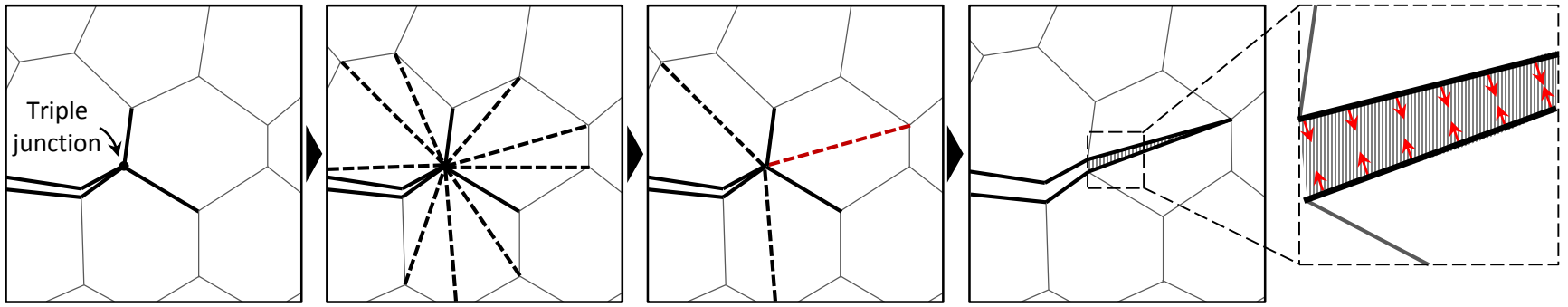

Leon SE*, Spring DW*, Paulino GH, Reduction in mesh bias for dynamic fracture using adaptive splitting of polygonal finite elements. *International Journal for Numerical Methods in Engineering*, Vol. 100, pp. 555-576, 2014.

Adaptive Refinement Operator for Reducing Mesh Bias

Additionally, we propose the use of an **adaptive refinement** operator, wherein each polygon around the crack tip is removed and replaced with a set of unstructured quads; which meet at the centroid of the original polygon.

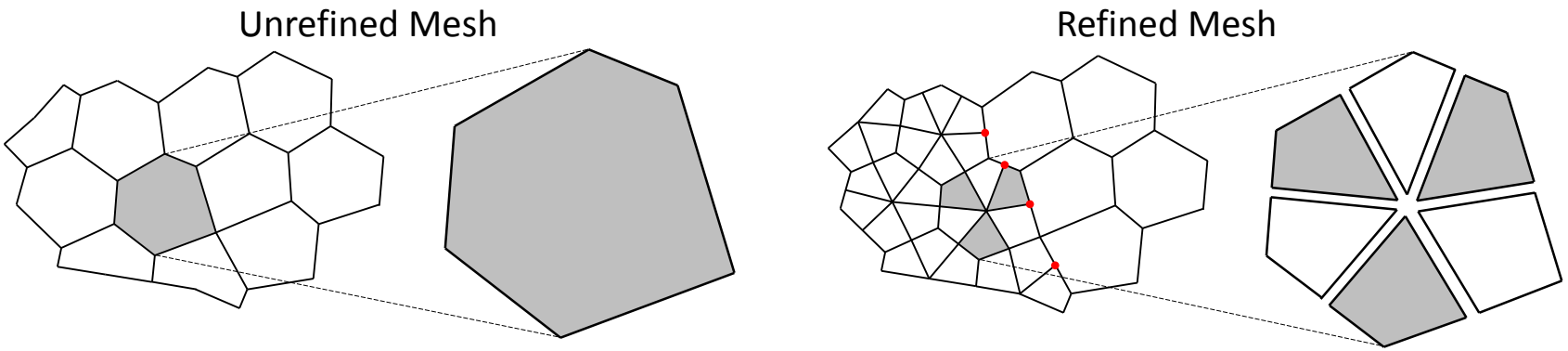

The mesh is adaptively refined in front of the propagating crack-tip.

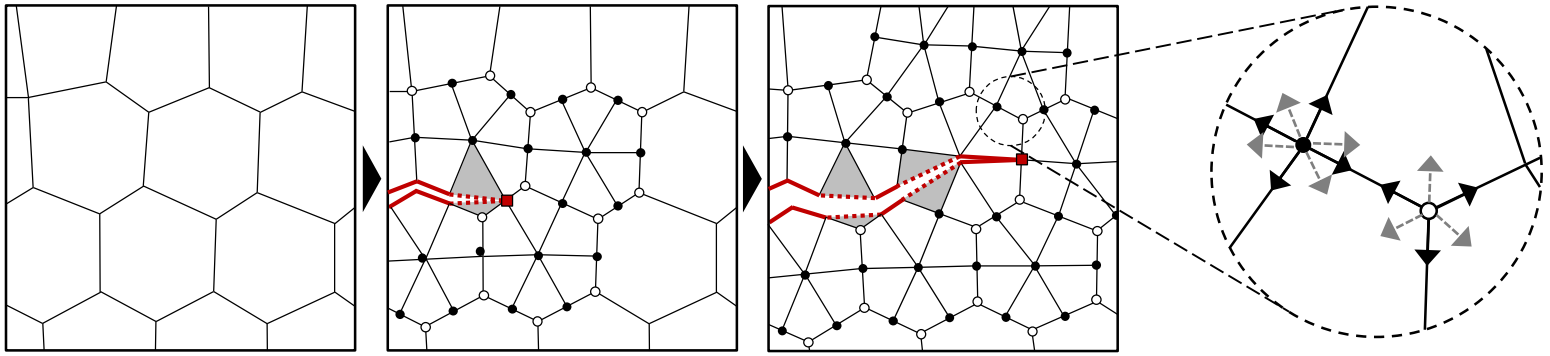

Spring DW, Leon SE, Paulino GH, Unstructured polygonal meshes with adaptive refinement for the numerical simulation of dynamic cohesive fracture. *International Journal of Fracture*, Vol. 189, pp. 33-57, 2014.

Quantification of Improvement in Path Deviation

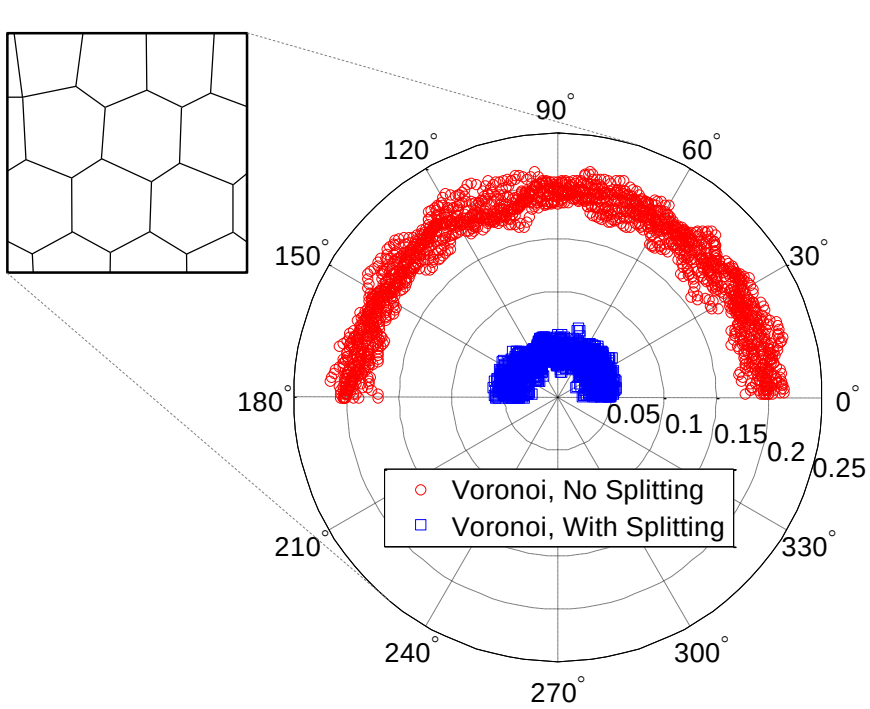

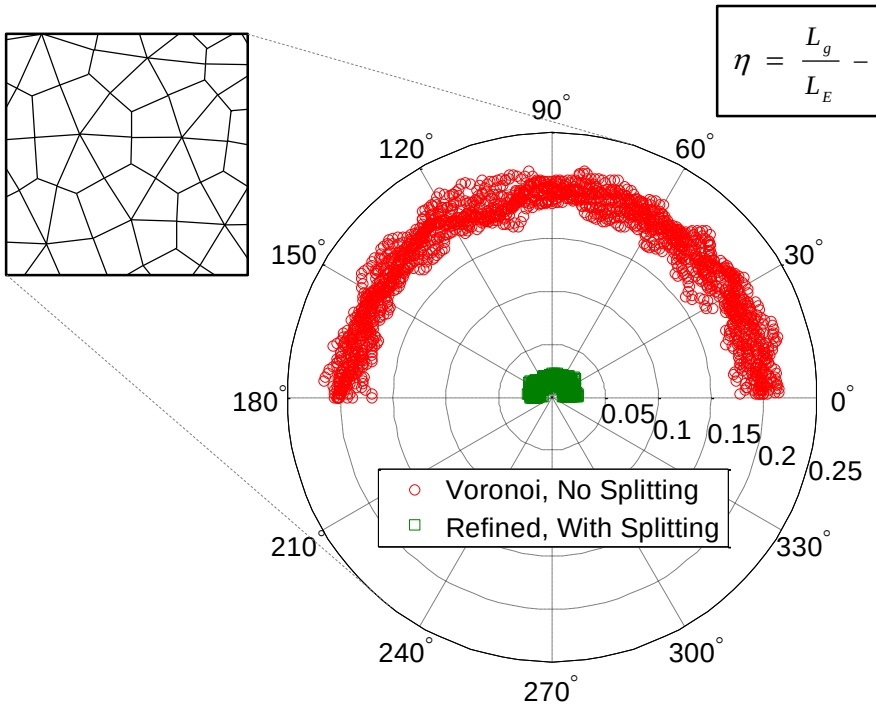

Meshing Strategy	Average	Standard Deviation	Improvement
Polygonal	0.1931	0.0013	-
Polygonal with Splitting	0.0445	0.0009	77%
Polygonal with Refinement	0.0698	0.0021	64%
Polygonal with Refinement and Splitting	0.0171	0.0004	91%

Leon SE*, Spring DW*, Paulino GH, Reduction in mesh bias for dynamic fracture using adaptive splitting of polygonal finite elements. *International Journal for Numerical Methods in Engineering*, Vol. 100, pp. 555-576, 2014.

Spring DW, Leon SE, Paulino GH, Unstructured polygonal meshes with adaptive refinement for the numerical simulation of dynamic cohesive fracture. *International Journal of Fracture*, Vol. 189, pp. 33-57, 2014.

Example: Dominant Crack with Microbranching

Experimental setup and results:

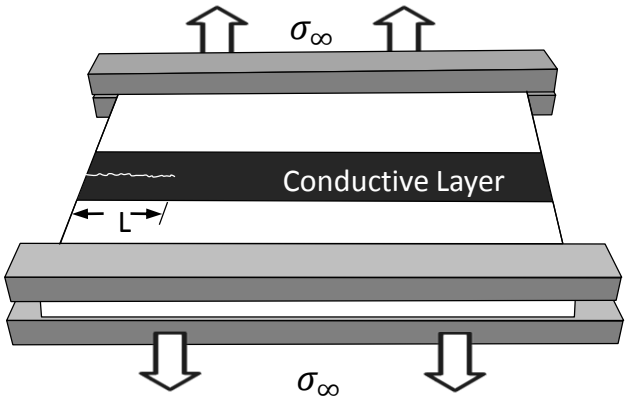

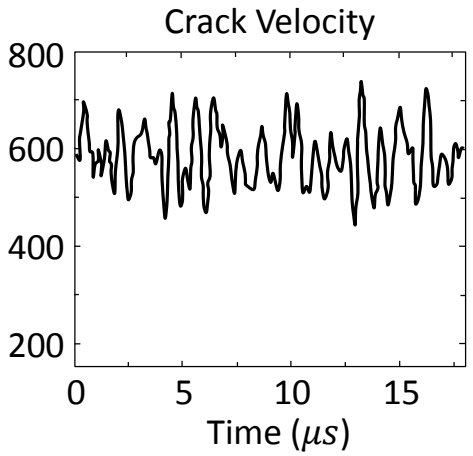

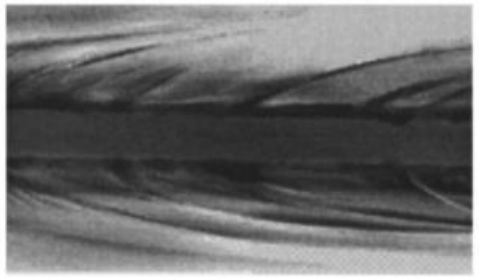

Numerical model:

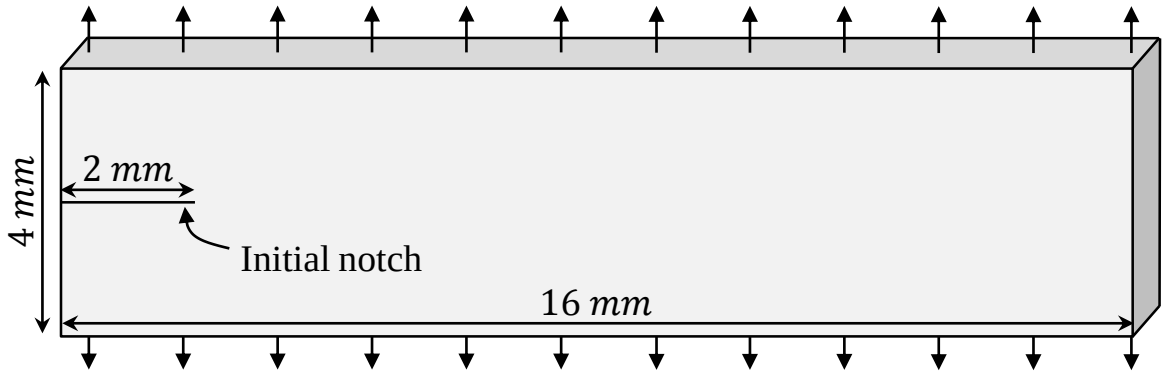

PMMA Properties

E	$3.24GPa$
ρ	$1190\,kg/m^3$
ϕ	$352.4\,N/m$
σ	$129.6MPa$
α	2

Sharon E, Fineberg J, Microbranching instability and the dynamic fracture of brittle materials. *Physical Review B*, vol. 54, pp. 7128-7139, 1996.

Spring DW, Leon SE, Paulino GH, Unstructured polygonal meshes with adaptive refinement for the numerical simulation of dynamic cohesive fracture. *International Journal of Fracture*, Vol. 189, pp. 33-57, 2014.

Fracture Patterns: Influence of Meshing Strategy

Adaptively refined unstructured meshes produce a smooth crack path with large macrobranches and a uniform distribution of microbranching.

Coarse Polygonal

Element-Splitting

Adaptively Refined

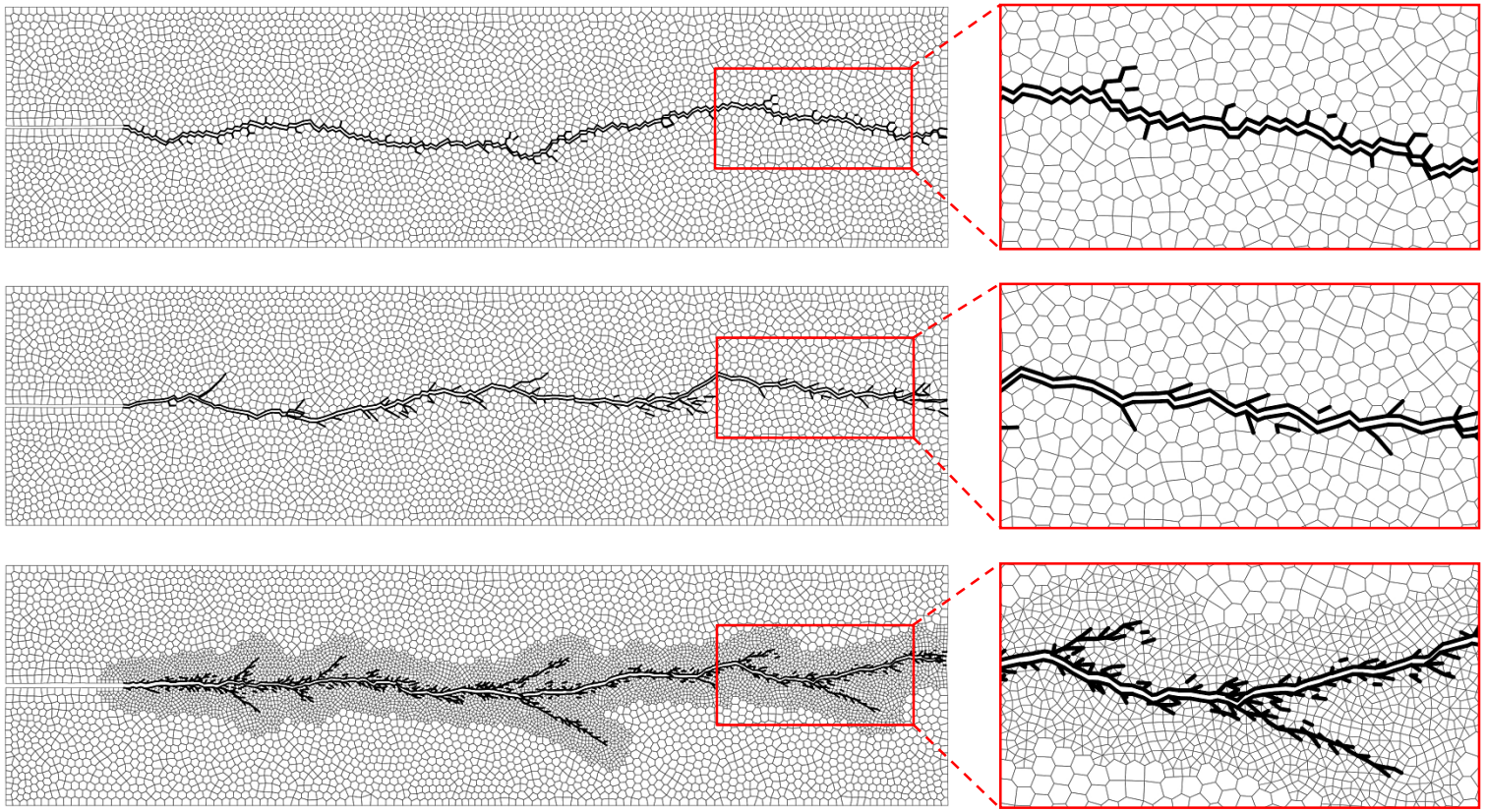

The adaptively refined meshes produce results in good agreement with experiments.

Spring DW, Leon SE, Paulino GH, Unstructured polygonal meshes with adaptive refinement for the numerical simulation of dynamic cohesive fracture. *International Journal of Fracture*, Vol. 189, pp. 33-57, 2014.

Influence of Meshing Strategy on the Crack-Tip Velocity

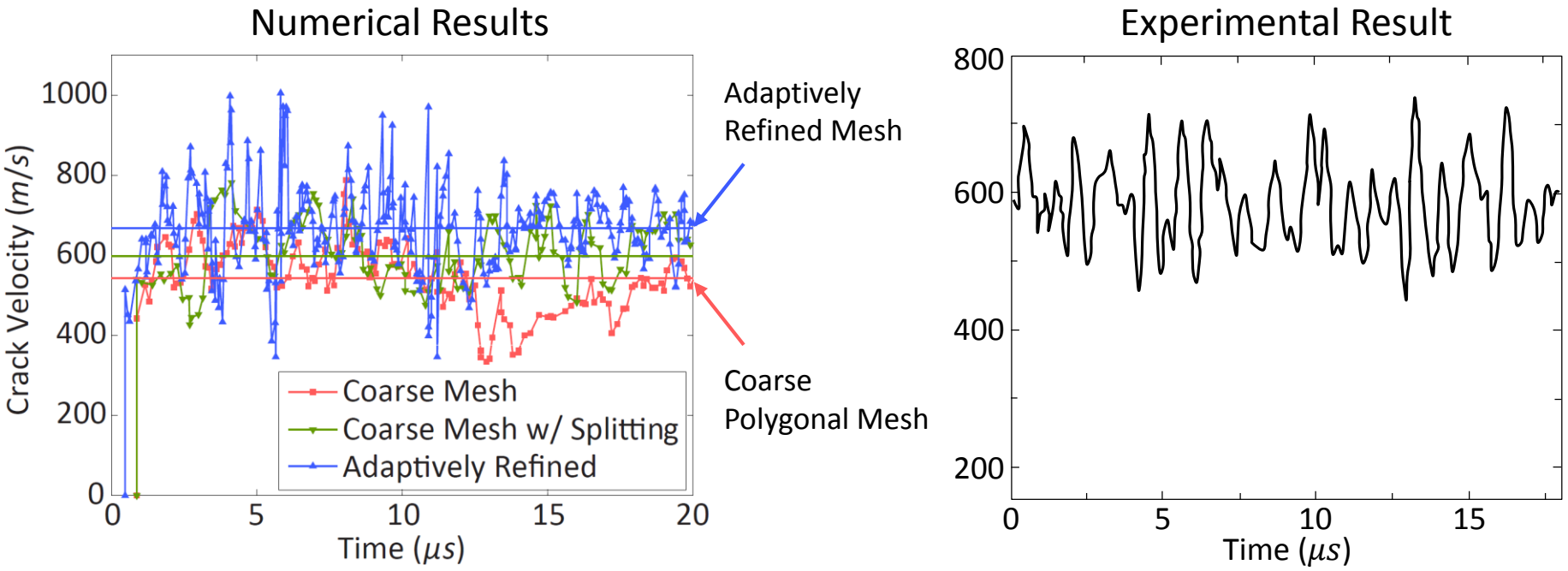

Sharon E, Fineberg J, Microbranching instability and the dynamic fracture of brittle materials. *Physical Review B*, vol. 54, pp. 7128-7139, 1996.

Spring DW, Leon SE, Paulino GH, Unstructured polygonal meshes with adaptive refinement for the numerical simulation of dynamic cohesive fracture. *International Journal of Fracture*, Vol. 189, pp. 33-57, 2014.

Comparison of Computational Cost

Case 1

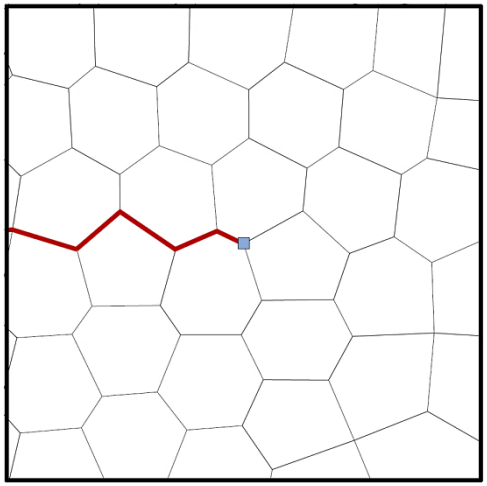

Polygonal

Case 2

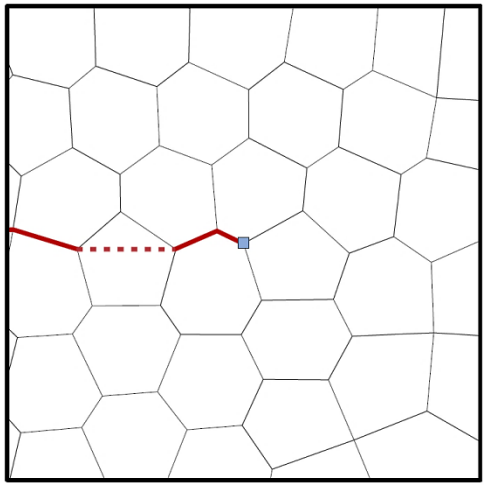

Element-Splitting

Case 3

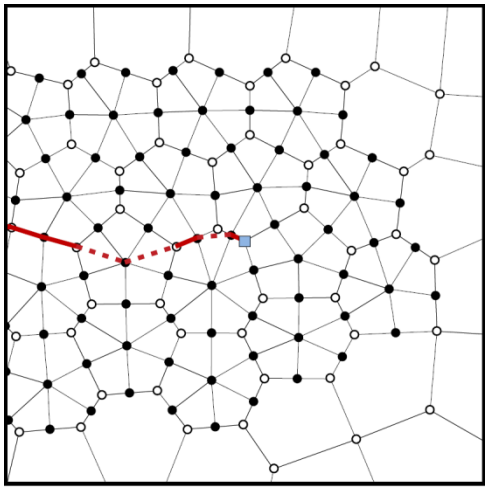

Adaptive Refinement

Case	Elements	Nodes	Cost (*min*)	Iterations to Fracture	Cost/Iteration (10^{-3} *s*)
1	4,000	7,188	21.5	28,200	45.7
2	4,000	7,188	20.8	23,000	54.3
3	4,000	7,188	19.1	21,000	54.6

Spring DW, Leon SE, Paulino GH, Unstructured polygonal meshes with adaptive refinement for the numerical simulation of dynamic cohesive fracture. *International Journal of Fracture*, Vol. 189, pp. 33-57, 2014.

Remarks

- Unstructured polygonal meshes produce an isotropic discretization of the problem domain.
- Without careful design considerations, polygonal meshes are inherently poorly suited to dynamic fracture simulation with the cohesive element method.
- The newly proposed topological operators are designed to increase the number of paths a crack can propagate along, and result in a meshing strategy on par with the best, fixed meshing strategy available in the literature.
- The adaptive refinement with element splitting scheme increases the problem size, but can decrease the computational cost.
- By combining geometrically and topologically unstructured methods, the model is truly random and reduces numerically induced restrictions. Thus, reducing uncertainty in numerical simulations.

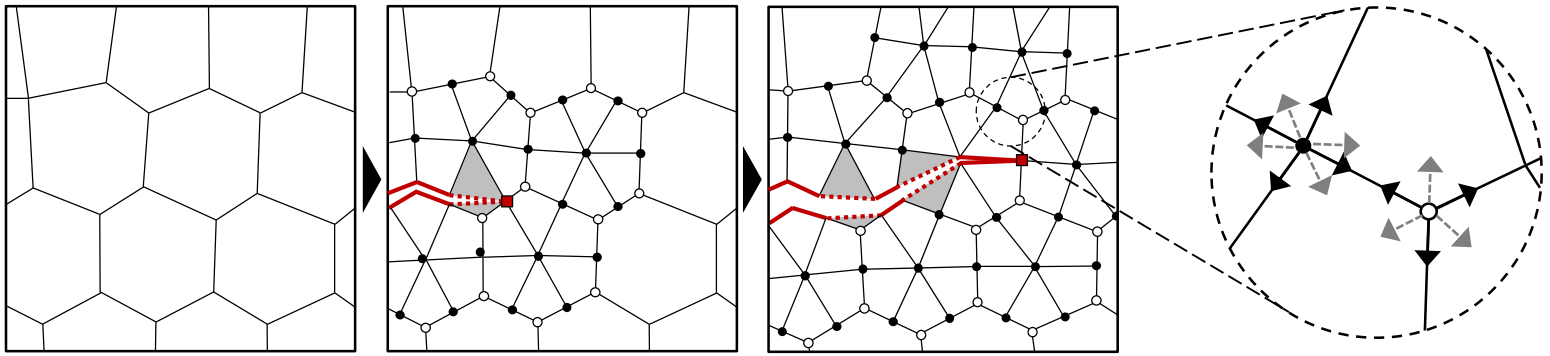

Leon SE*, Spring DW*, Paulino GH, Reduction in mesh bias for dynamic fracture using adaptive splitting of polygonal finite elements. *International Journal for Numerical Methods in Engineering*, Vol. 100, pp. 555-576, 2014.

Spring DW, Leon SE, Paulino GH, Unstructured polygonal meshes with adaptive refinement for the numerical simulation of dynamic cohesive fracture. *International Journal of Fracture*, Vol. 189, pp. 33-57, 2014.

Presentation Structure

1. Perfectly Bonded Interphases in Particle Reinforced Elastomers

- Goudarzi T, **Spring DW**, Paulino GH, Lopez-Pamies O, Filled elastomers: A theory of filler reinforcement based on hydrodynamic and interphasial effects. *Journal of the Mechanics and Physics of Solids*, Vol. 80, pp. 37-67, 2015

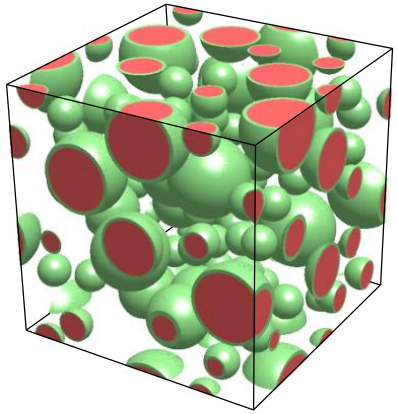

2. Interfacial Debonding in Particle Reinforced Elastomers

- **Spring DW**, Paulino GH, A growing library of three-dimensional cohesive elements for use in ABAQUS. *Engineering Fracture Mechanics*, Vol. 126, pp. 190-216, 2014.
- **Spring DW**, Paulino GH, Computational homogenization of the debonding of particle reinforced elastomers: The role of interphases in interfaces. *Under Review.*

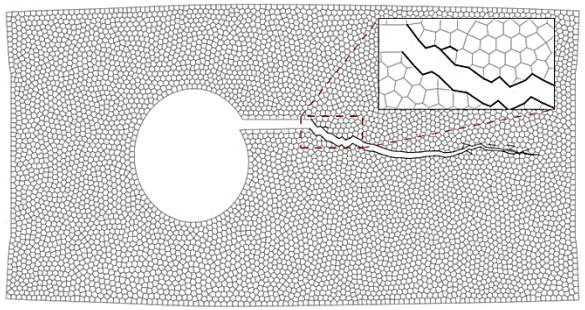

3. Reducing Mesh Bias in Dynamic Fracture Simulations Through Adaptive Operators

- Leon SE, **Spring DW**, Paulino GH, Reduction in mesh bias for dynamic fracture using adaptive splitting of polygonal finite elements. *International Journal for Numerical Methods in Engineering*, Vol. 100, pp. 555-576, 2014.
- **Spring DW**, Leon SE, Paulino GH, Unstructured polygonal meshes with adaptive refinement for the numerical simulation of dynamic cohesive fracture. *International Journal of Fracture*, Vol. 189, pp. 33-57, 2014.

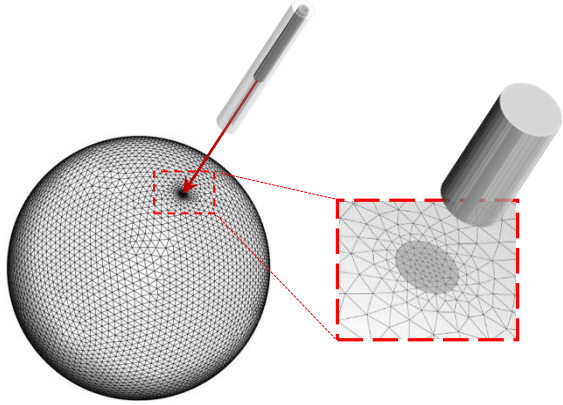

4. Regularizing Pervasive Fracture and Fragmentation Behavior in Three-Dimensions

- **Spring DW**, Paulino GH, Numerical unstructuring as a means for achieving pervasive fracture and fragmentation in three-dimensions. *In Preparation*.

Pervasive Fracture and Fragmentation in 3D

Pervasive cracking and fragmentation comprises the entire spectrum of fracture behavior.

Characteristics

- Crack branching
- Crack coalescence
- Complete fragmentation

Issues

- Sensitivity to material heterogeneity
- Any structure introduced to the mesh will bias fragmentation behavior

Similar to our study of mesh bias in 2D dynamic fracture, we developed a 3D dynamic fracture code to investigate these issues in pervasive fragmentation.

Spring DW, Paulino GH, Numerical unstructuring as a means for achieving pervasive fracture and fragmentation in three-dimensions. *In Preparation*.

Sensitivity to Material Heterogeneity

- Most materials contain heterogeneity (or defects) at the microscale.

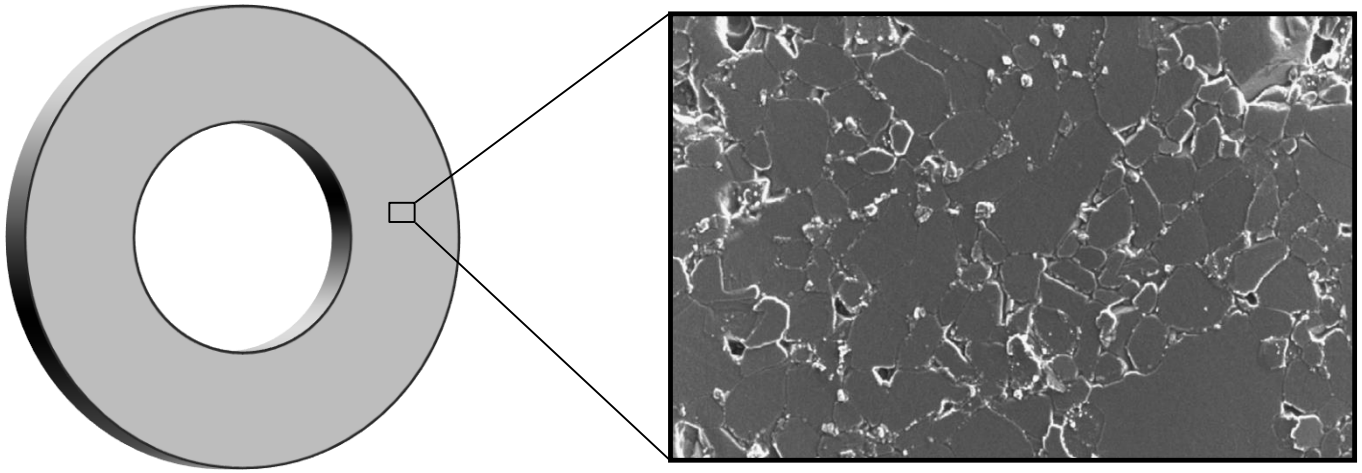

- Defects naturally arise in materials due to grain boundaries, voids, or inclusions.
- Defects may also be introduced through the act of processing or machining the material.
- Microscale defects constitute potential regions where stresses can concentrate and lead to damage or failure.

Weibull W, 1939. A statistical theory of the strength of materials, *Proceedings of the Royal Academy of Engineering Sciences,* Vol. 151, pp. 1–45.

Constitutively Unstructured Through a Statistical Distribution of Material Properties

The material strength is assumed to follow a modified Weibull distribution:

$$\sigma = \sigma_{min} + \lambda\left(-\ln(1-\rho)\right)^{1/m}$$

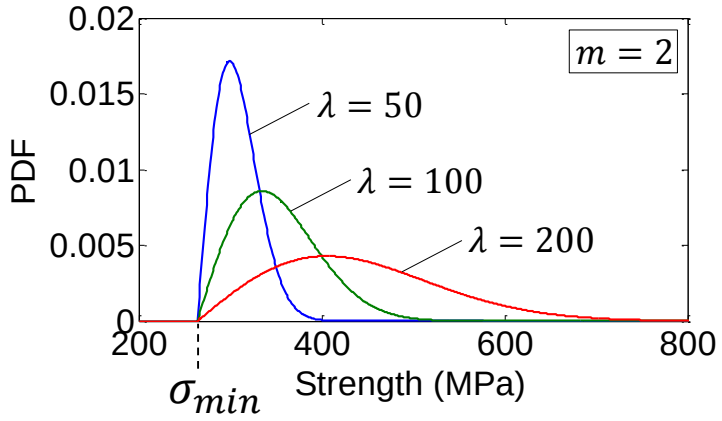

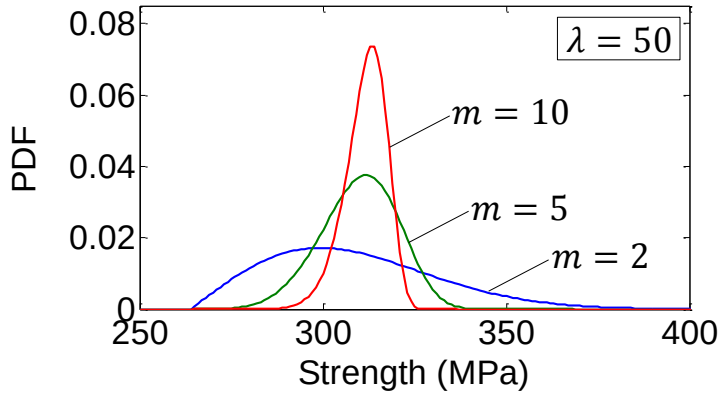

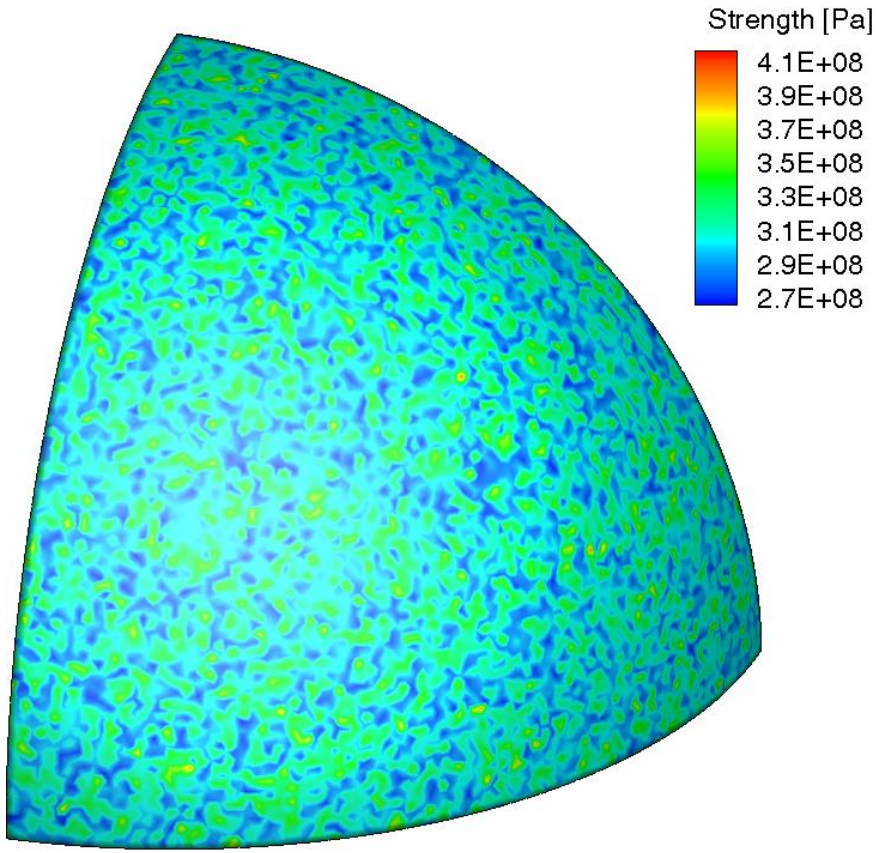

$\sigma_{min} = 264MPa, \lambda = 50,\ m = 2$

Weibull W, 1939. A statistical theory of the strength of materials, *Proceedings of the Royal Academy of Engineering Sciences,* Vol. 151, pp. 1–45.

Structured Artifacts in Automatically Generated Meshes

- Automatic mesh generators often conduct additional post-processing of the mesh; to remove elements with degenerate edges and sliver elements.
- In some cases, this additional post-processing leads these (initially random) meshes to contain an underlying structure.

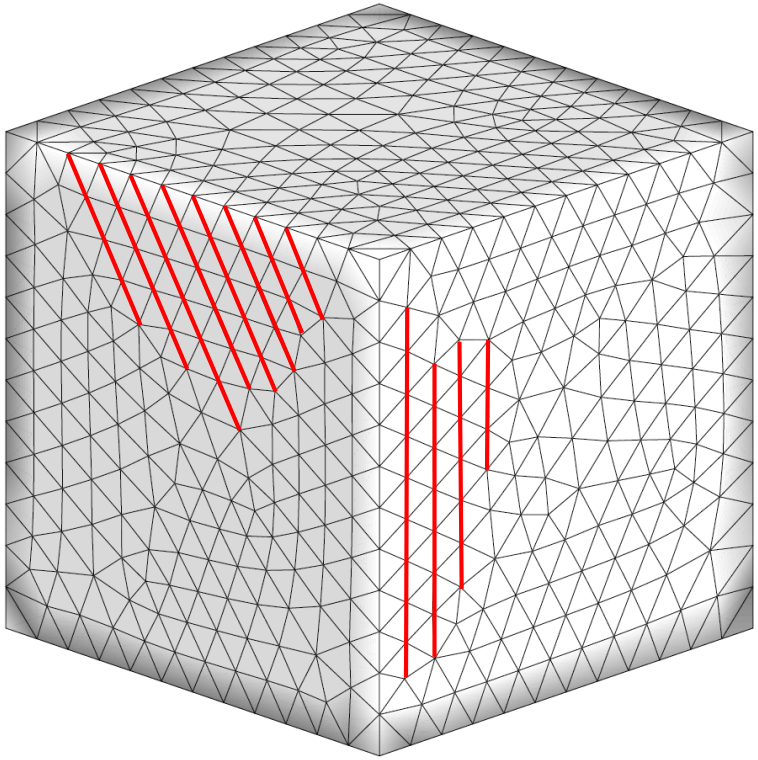

- To remove this structure, we propose using the technique of nodal perturbation.

Spring DW, Paulino GH, Numerical unstructuring as a means for achieving pervasive fracture and fragmentation in three-dimensions. *In Preparation*.

Geometrically Unstructured Through Nodal Perturbation

Nodal Perturbation:

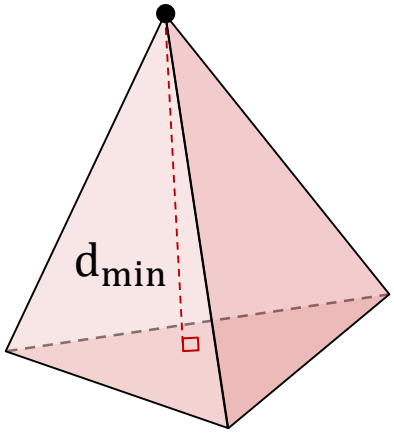

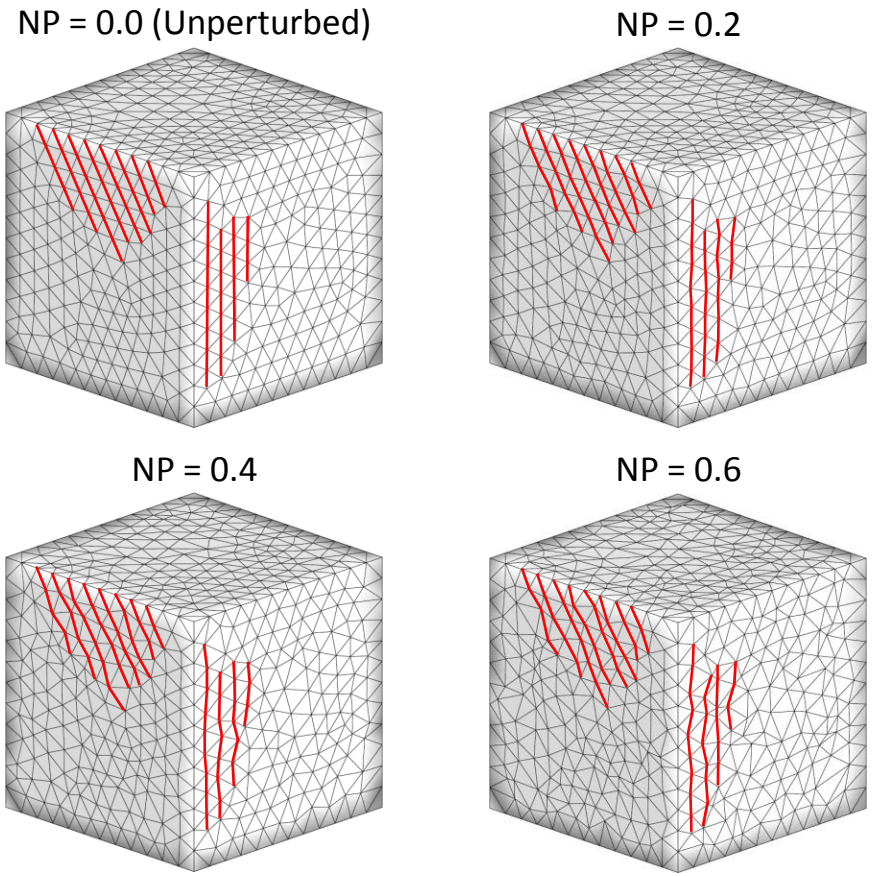

- Nodes are randomly perturbed by a multiple of d_{min}:

$$\mathbf{X}_n = \mathbf{X}_o + d_{min} \times NP \times \mathbf{n}_{random}$$

- We conduct a set of geometric studies to quantify the effect of the magnitude of the nodal perturbation factor on the quality of the mesh.
- Our investigation indicates that a nodal perturbation factor of 0.4 is most suited to 3D meshes – producing a high level of unstructuredness, while maintaining element quality.

Spring DW, Paulino GH, Numerical unstructuring as a means for achieving pervasive fracture and fragmentation in three-dimensions. *In Preparation*.

Example: Radial Fragmentation of a Hollow Sphere

Here, we consider the pervasive fragmentation of a hollow sphere with symmetric boundary conditions.

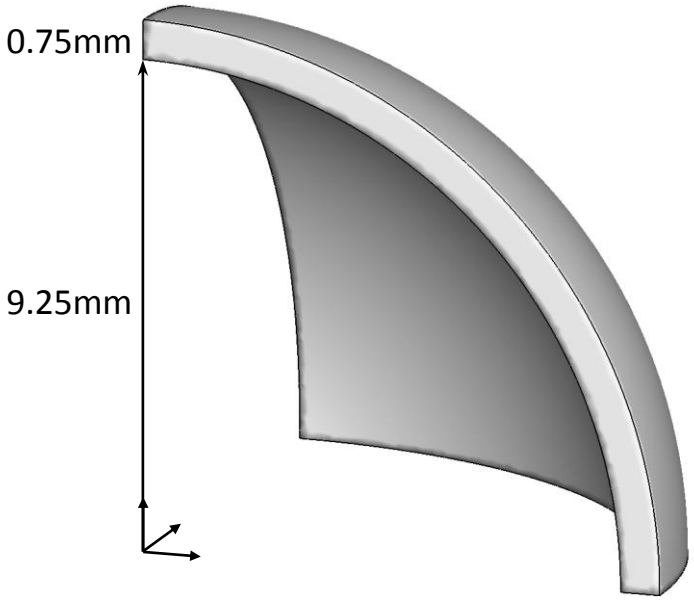

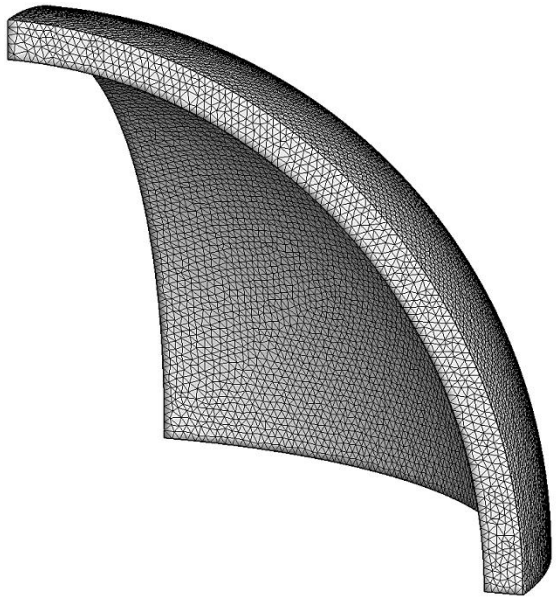

$E = 370\ GPa \quad \rho = 3900\ kg/m^3$
$\phi = 50\ J/m^2 \quad \sigma_{min} = 264\ MPa$

~100,000 Elements
~25,000 Nodes

The sphere is impacted with an impulse load, which is converted to an initial nodal velocity

$$\mathbf{v_0}(x, y, z) = \dot{\varepsilon}\mathbf{x}$$

Sarah Levy, "Exploring the physics behind dynamic fragmentation through parallel simulations." PhD. Dissertation, Ecole Polytechnique Federale de Lausanne, 2010.

Spring DW, Paulino GH, Numerical unstructuring as a means for achieving pervasive fracture and fragmentation in three-dimensions. *In Preparation*.

Regularization Through Geometric Features

We investigate the influence of idealized surface features, namely bumps and dimples, on the fragmentation behavior of the hollow sphere.

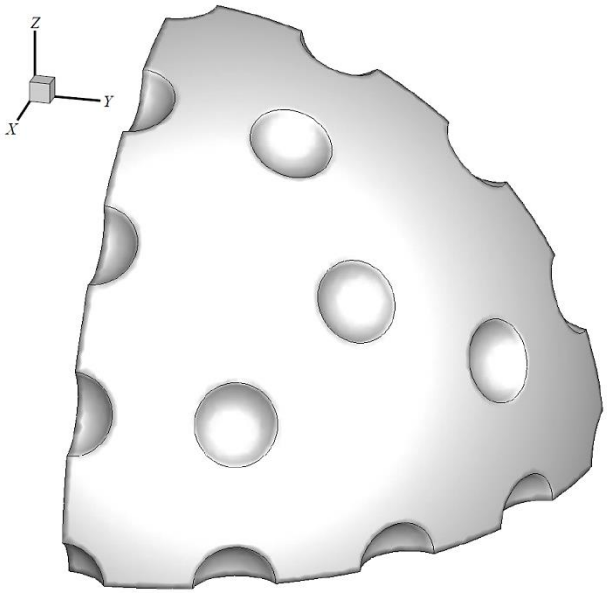

Dimples or Depressions

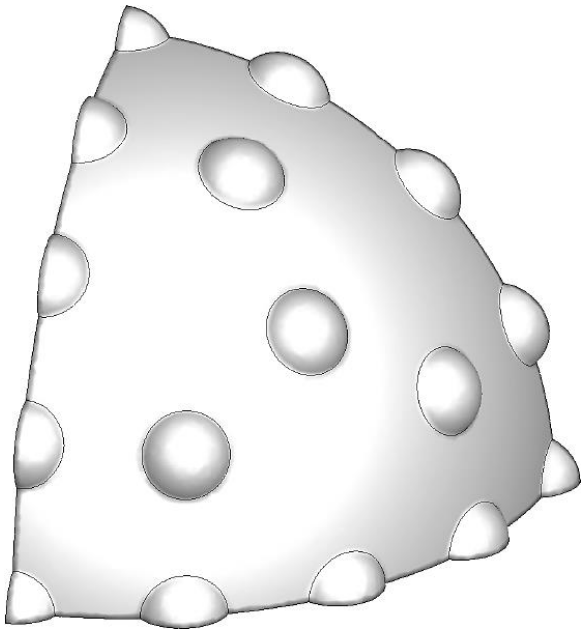

Bumps or Protrusions

Spring DW, Paulino GH, Numerical unstructuring as a means for achieving pervasive fracture and fragmentation in three-dimensions. *In Preparation*.

Geometric Features Can Be Used to Regularize Fragmentation Patterns

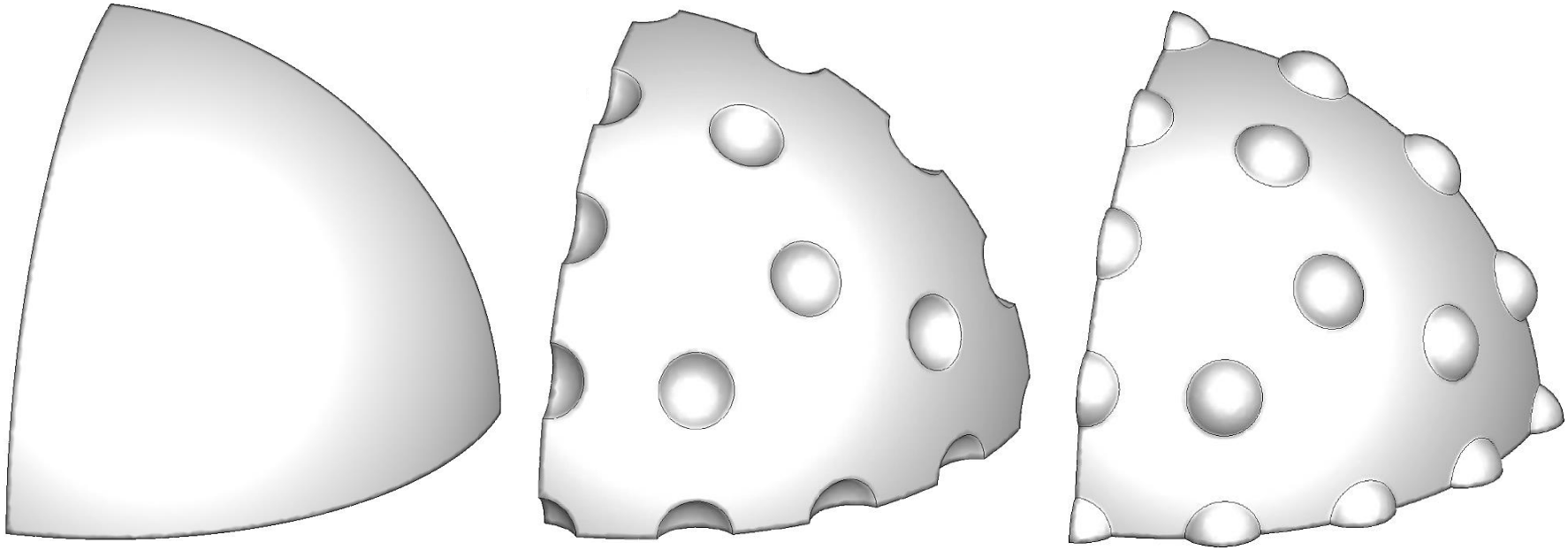

Smooth Dimples Bumps

- The initial impact velocity is set at: $\mathbf{v}_0(x, y, z) = 2500\mathbf{x}$
- Similar trends are observed at higher impact velocities and with different statistical distributions of material strength.

Spring DW, Paulino GH, Numerical unstructuring as a means for achieving pervasive fracture and fragmentation in three-dimensions. *In Preparation*.

Example: Kidney Stone Fragmentation by Direct Impact

This example considers the direct impact of a kidney stone. We use this example to investigate the use functionally graded materials to regularize fragmentation behavior.

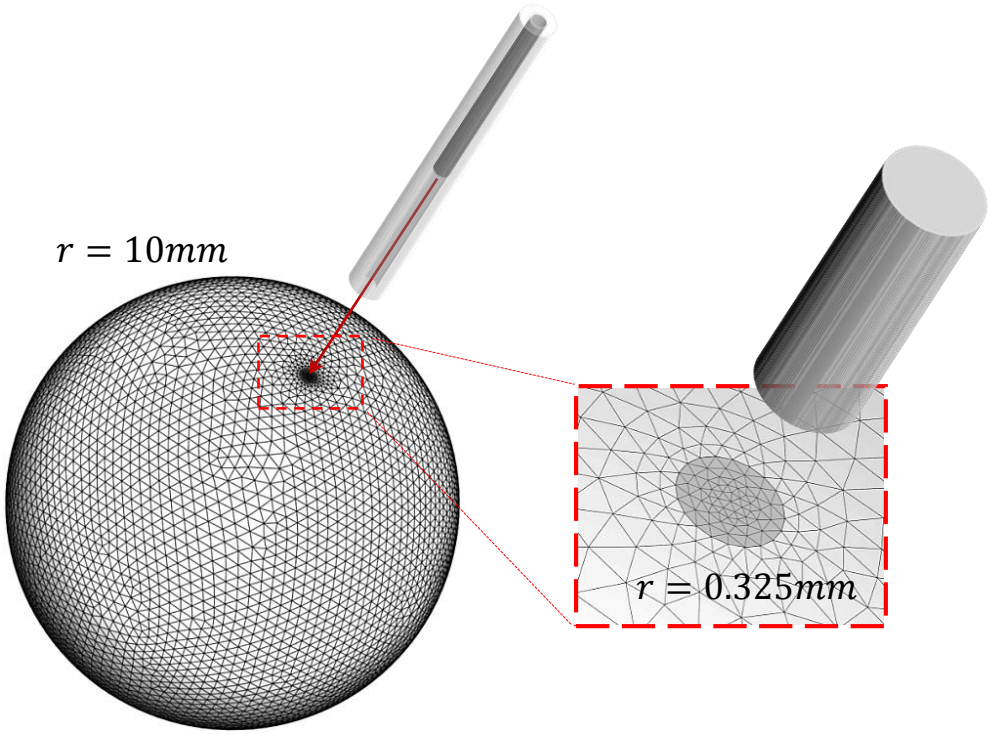

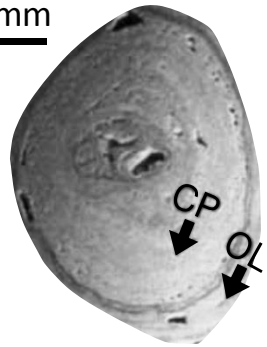

CP = Core Part
OL = Outer Layer

Materials considered:

COM: $E = 25.16\ GPa$ $\rho = 2038\ kg/m^3$
$\phi = 0.735\ J/m^2$ $\sigma = 1.0\ MPa$

CA: $E = 8.504\ GPa$ $\rho = 1732\ kg/m^3$
$\phi = 0.382\ J/m^2$ $\sigma = 0.5\ MPa$

COM: calcium oxalate monohydrate
CA: carbonate apatite

Spring DW, Paulino GH, Numerical unstructuring as a means for achieving pervasive fracture and fragmentation in three-dimensions. *In Preparation*.

Caballero A, Molinari JF, Finite element simulations of kidney stones fragmentation by direct impact: Tool geometry and multiple impacts. *International Journal of Engineering Science*, vol. 48, pp. 253-264, 2010.

Zhong P, Chuong CJ, Goolsby RD, Preminger GM, Microhardness measurements of renal calculi: Regional differences and effects of microstructure. *Journal of Biomedical Materials Research*, vol. 26, pp. 1117-1130, 1992.

Fragmentation of a Homogeneous Stone

To develop a baseline, we first consider the fragmentation of a homogeneous stone with different levels of variation in material properties.

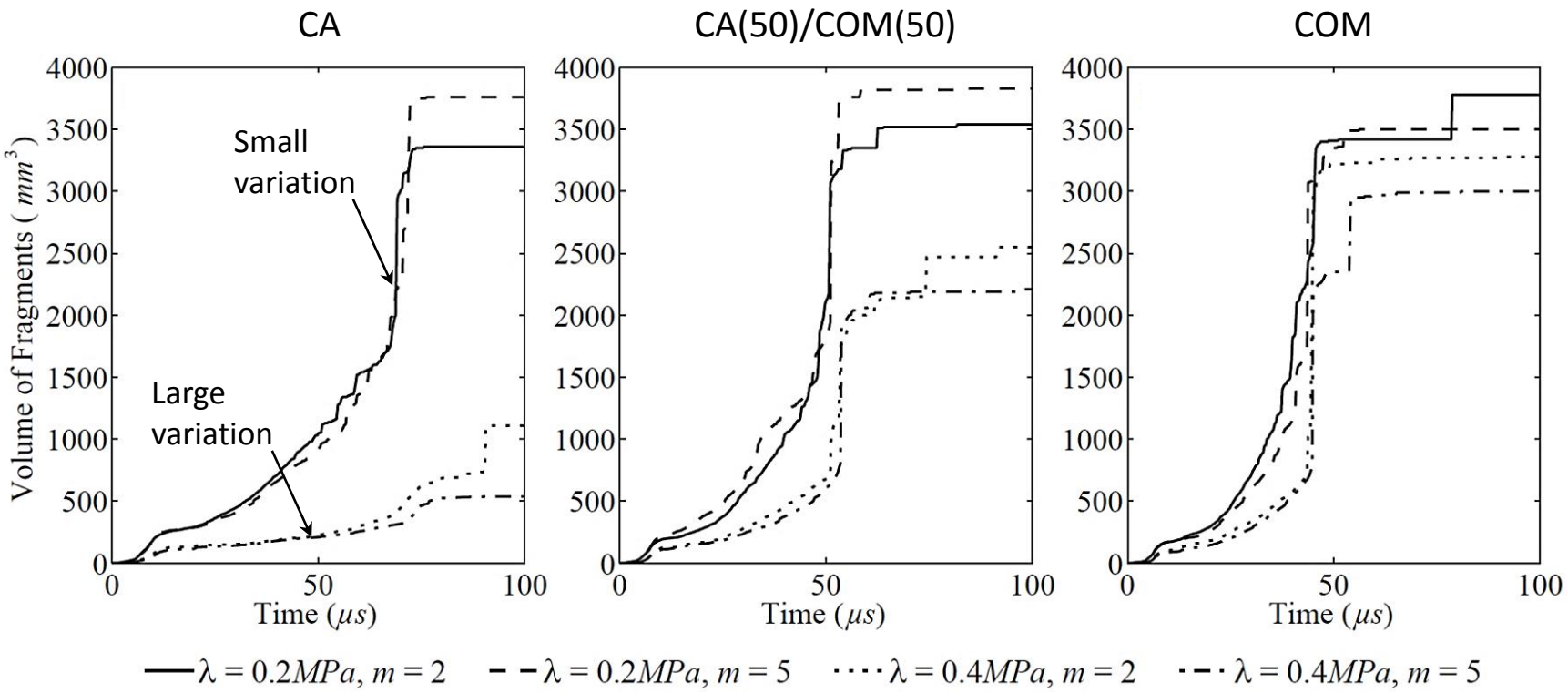

CA: $E = 8.504\ GPa$ $\rho = 1732\ kg/m^3$ $\phi = 0.382\ J/m^2$ $\sigma = 0.5\ MPa$

COM: $E = 25.16\ GPa$ $\rho = 2038\ kg/m^3$ $\phi = 0.735\ J/m^2$ $\sigma = 1.0\ MPa$

Spring DW, Paulino GH, Numerical unstructuring as a means for achieving pervasive fracture and fragmentation in three-dimensions. *In Preparation*.

Fragmentation of a Functionally Graded Stone

Next, we show that fragmentation behavior can be regularized by modelling the graded distribution of material in the stone.

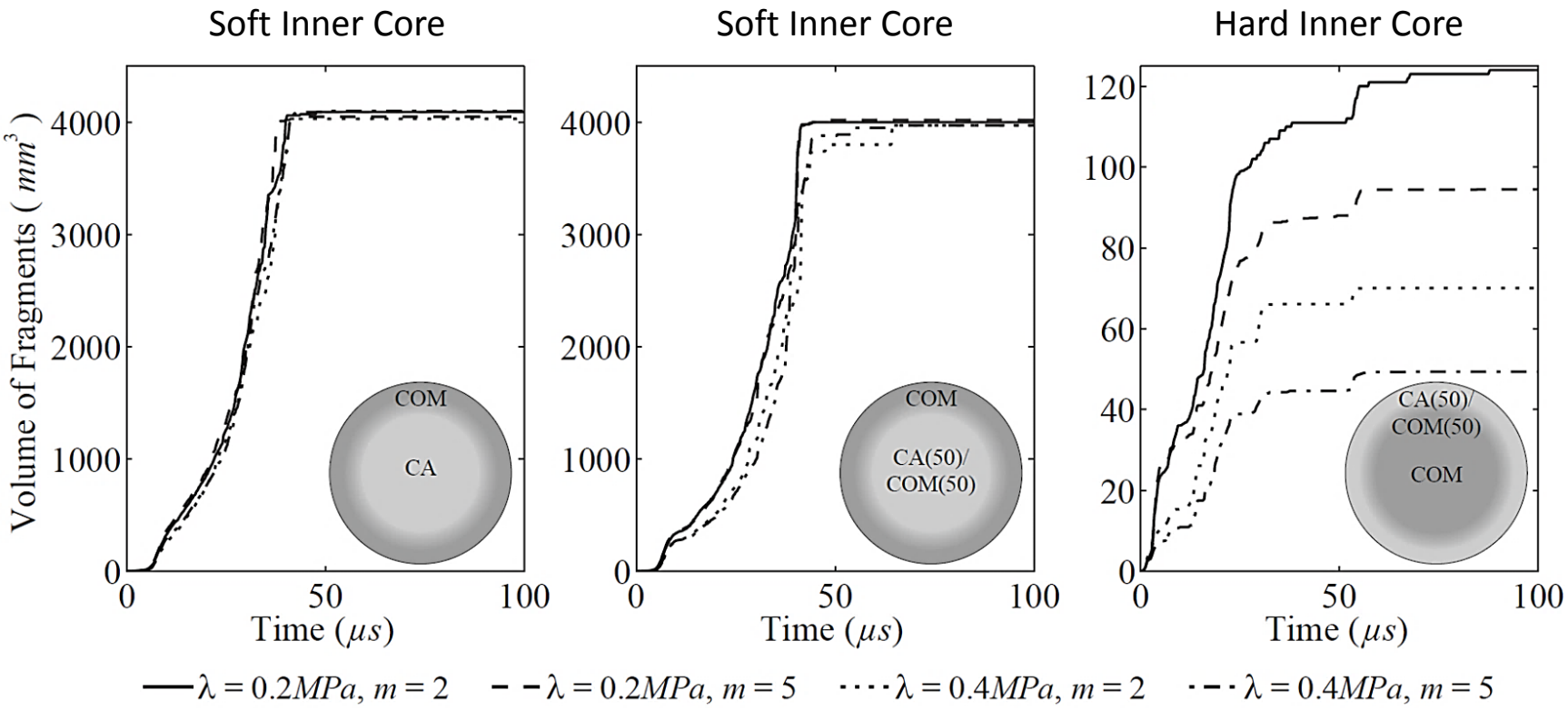

CA: $E = 8.504\ GPa$ $\rho = 1732\ kg/m^3$ $\phi = 0.382\ J/m^2$ $\sigma = 0.5\ MPa$

COM: $E = 25.16\ GPa$ $\rho = 2038\ kg/m^3$ $\phi = 0.735\ J/m^2$ $\sigma = 1.0\ MPa$

Spring DW, Paulino GH, Numerical unstructuring as a means for achieving pervasive fracture and fragmentation in three-dimensions. *In Preparation*.

Remarks

- The cohesive element method constitutes a framework which allows us to capture the full spectrum of fracture mechanisms.
- A statistical distribution of material properties can be used to account for microscale defects and inhomogeneities.
- A random perturbation of the nodes reduces structure created by automatic mesh generators.
- By incorporating constitutive and geometric heterogeneity in the model we can reduce numerically induced artifacts into the simulated results and increase the certainty in our simulations.
- We can use simple geometric and constitutive design features to regularize pervasive fracture and fragmentation behavior in three-dimensions.

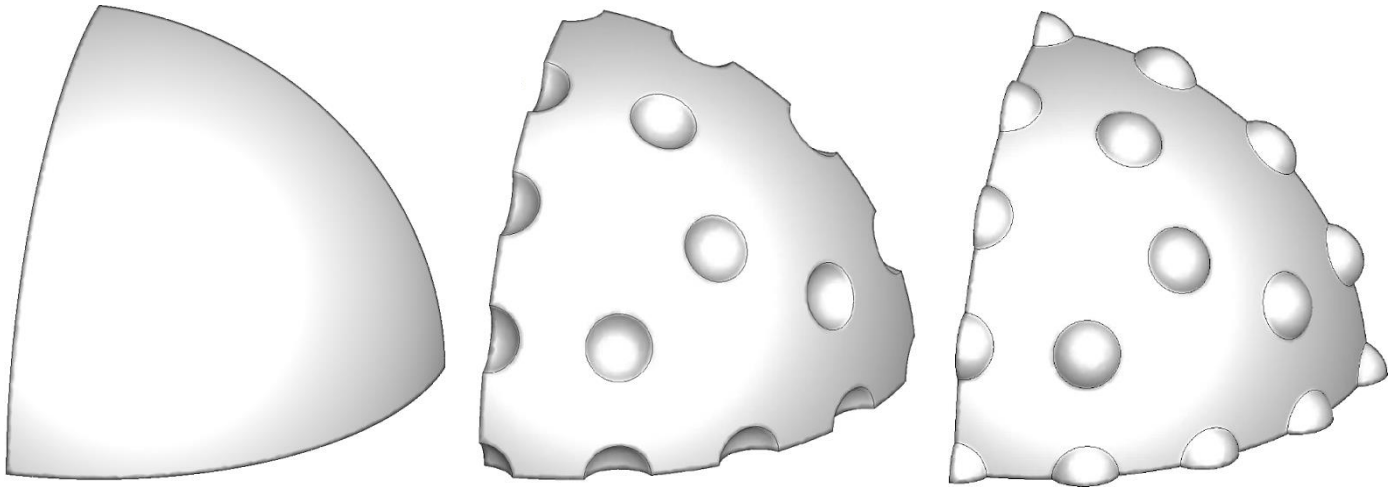

Spring DW, Paulino GH, Numerical unstructuring as a means for achieving pervasive fracture and fragmentation in three-dimensions. *In Preparation*.

Contributions

Discussed in this presentation:

- Goudarzi T, **Spring DW**, Paulino GH, Lopez-Pamies O, Filled elastomers: A theory of filler reinforcement based on hydrodynamic and interphasial effects. *Journal of the Mechanics and Physics of Solids*, Vol. 80, pp. 37-67, 2015.
- **Spring DW**, Paulino GH, Computational homogenization of the debonding of particle reinforced elastomers: The role of interphases in interfaces. *Under Review*.
- **Spring DW**, Leon SE, Paulino GH, Unstructured polygonal meshes with adaptive refinement for the numerical simulation of dynamic cohesive fracture. *International Journal of Fracture*, Vol. 189, pp. 33-57, 2014.
- **Spring DW**, Paulino GH, Numerical unstructuring as a means for achieving pervasive fracture and fragmentation in three-dimensions. *In Preparation*.

Not covered in this presentation:

- **Spring DW**, Paulino GH, A growing library of three-dimensional cohesive elements for use in Abaqus. *Engineering Fracture Mechanics*, Vol. 126, pp. 190-216, 2014.
- Leon SE*, **Spring DW***, Paulino GH, Reduction in mesh bias for dynamic fracture using adaptive splitting of polygonal finite elements. *International Journal for Numerical Methods in Engineering*, Vol. 100, pp. 555-576, 2014.
- Hasemi R*, **Spring DW***, Paulino GH, On small deformation interfacial debonding in composite materials containing multi-coated particles. *Journal of Composite Materials*, Published Online, 2015.
- **Spring DW**, Paulino GH, On the thermodynamic consistency of the Park-Paulino-Roesler cohesive model. *Under Review*.
- Amirkhanian AN, **Spring DW**, Roesler JR, Paulino GH, Forward and inverse analysis of concrete fracture using the disk-shaped compact tension test. *Journal of Testing and Evaluation,* Accepted.

Acknowledgements

- **Advisor**: Glaucio H. Paulino
- **Committee members**: Iwona Jasiuk, William Buttlar, Oscar Lopez-Pamies, Ahmed Elbanna, Kyoungsoo Park
- **Collaborators**: Oscar Lopez-Pamies, Taha Goudarzi, Sofie Léon, Armen Amirkhanian, Jeffery Roesler
- **Additional Friends and Colleagues**: Heng Chi, Evgueni Filipov, Arun L. Gain, Oliver Giraldo-Londoño, Tomás Zegard, Cameron Talischi, Junho Song, Lauren Beghini, Ke (Chris) Liu, Xiaojia (Shelly) Zhang, Tuo Zhao, Emily Daniels, Tam Nguyen, Marco Alfano, Yang Jiang, Will Colletti, Eshan Dave, Rodrigo Espinha, Ludimar Lima de Aguiar, Luis Arnaldo, Peng Wei, Hélio Emmendoerfer Junior, Rejane Canha, and Leonardo Duarte
- **Funding Agencies**: NSERC, UIUC and NSF

Thank You, Questions?

Daniel Spring

spring2@illinois.edu